Development and Control of Modular Robots for Rough Terrain Traversal

Thesis submitted in partial fulfillment
of the requirements for the degree of

MS by Research
in
Computer Science and Engineering

by

Avinash Siravuru
201107641
avinash.siravuru@research.iiit.ac.in

Robotics Research Centre
International Institute of Information Technology
Hyderabad - 500 032, INDIA
July 2014

International Institute of Information Technology
Hyderabad, India

CERTIFICATE

It is certified that the work contained in this thesis, titled "Development and Control of Modular Robots for Rough Terrain Traversal" by Avinash Siravuru, has been carried out under my supervision and is not submitted elsewhere for a degree.

_____ _____

Date Adviser-1: Prof. K Madhava Krishna

_____ _____

Date Adviser-2: Prof. Suril V Shah

To The Teacher and The Force.

Acknowledgments

I want to acknowledge my advisers Dr. Madhava Krishna and Dr. Suril V Shah for their unstinting support during the evolution of this thesis. I also wish to thank all my colleagues from the Robotics Research Center for being my punching bags, lab rats, mentors and everything in between. Particularly, I want to thank Arun Kumar Singh and Anurag V V for their innovative and inspiring ideas during the formative stages of this project. I am equally grateful to Akshaya Purohit, Ankur Srivastava, Priya Bansal and Shivraj for helping me build the prototype and rigorously test it. The roles of Snehal Gandham, Venkat Ramesh have been equally critical and timely for testing the wheel-torque controller, and I heartily thank them for the same.

Harsha Turlapati, Phani and Naren Nayak are the chosen few who will take this project forward into more uncharted and bumpy territories, where no robot has gone before. Not only do I thank them for adopting my baby, but also wish them the very best for their future endeavors. I have had the most fruitful time of my life at the Robotics Research Center and I cherish every single moment of it, the good, the bad and the ugly. Therefore I am very grateful to IIIT-Hyderabad for providing me the best people and infrastructure to solve pertinent problems and do my bit in helping robots eventually take over our world!

Abstract

In this thesis, the development of a novel compliant modular robot is proposed for deployment in Urban Search And Rescue(USAR) scenarios. In the light of the recent natural disasters in India and Japan, there is a renewed interest in developing rough terrain robots that can aid in search and rescue efforts by navigating through the rubble to search for trapped victims and dispense basic first-aid. Specifically, USAR scenarios are very challenging for robots. Each disaster is unique and the terrain knowledge gained from one may not be useful in the other. Additionally, the obstacles are so varied in size, shape and rigidity that a conventional single block mobile robot is often limited by either its size or its limited internal freedom to deform enough along these obstacles.

Keeping this in view, we propose the use of a modular design. Each robot module consists of a link and a wheel pair, that are capable of traversing on their own. The wheels are powered to provide propulsion for the robot. The modules are combined to form a snake-like structure and a joint, called link joint, is created between every module pair to allow free rotation (pitch) in the sagittal plane. In the literature, these type of robots are called snake-like robots and more specifically Active Wheel-Passive Joint (AW-PJ) type of robots. These robots typically have a passive articulation mechanism due to the absence of motors at the link joints. While these robots have better ability to navigate through tight pockets, they cannot climb heights greater than one module length due to the problem of tip-over. The primary motivation of this thesis is to enable these robots to climb bigger obstacles and develop a methodology to estimate the number of modules required to climb any given height. This enables us to add more modules, when required, and in principle, climb any given height.

Initial work focused on the development of a semi-active modular robot. The robot had five modules and it was minimally equipped with two motors, one each at the second and fourth link joints, respectively. The idea was to use the passive mechanism for climbing steps of smaller heights and motor only while climbing steps of bigger heights. A model-based controller was designed for the active link joints to achieve big-step climbing. The robot therefore had the advantage of height-independent climbing motion as in the case of passive mechanism along with the extra freedom of active joints for maintaining vehicle stability, when necessary. Efficacy of

the mechanism was exhibited through simulations on steps of various heights. However, it was realized that this approach was useful to climb heights only upto twice the individual module length. To climb bigger heights, the robot would need motors at all its link joints, leading to a more bulkier design. Motors at the link joints are also known to be susceptible to damage due to impact loads during traversal, making such designs less durable.

In order to overcome this disadvantage, the use of compliant joints is proposed. Motors are no longer used at the link joints for posture control. Instead, springs are designed such that they are stiff enough to restrict modules from tipping over while offering sufficient compliance to maneuver on uneven terrains. Spring stiffness for such joints is estimated by formulating an optimization problem over the static equilibrium equations of the robot. The optimization objective is to minimize all link joint moments at every instant of its climbing maneuver. This is one of the key novelties of the proposed work. A design methodology is also proposed for developing an n-module compliant robot for climbing given height on a surface with prescribed coefficient of friction. The performance of the proposed formulation is illustrated for climbing big obstacles and traversing uneven terrains, using both numerical and experimental validation on 3- and 5-module robots. The robot is successfully able to climb maximum heights of 17 cm and 36 cm using 3 and 5 modules, respectively.

As a secondary contribution, an optimal wheel-torque based controller is developed to minimize wheel slip. This helps in reducing odometric error and maximizing energy efficiency. Wheel actuators are the only actively controllable elements of this robot, as the modules are connected using passive compliant joints. Wheel-slip offers a lot of hindrance while traversing on uneven terrains. Therefore, minimizing wheel-slip is crucial to augment its performance. Here, the optimization objective is to minimize the traction-to-normal force ratios at all the wheels. It is shown both numerically and experimentally that the proposed controller not only minimizes slip but also reduces the mean torque requirement for traversing on uneven terrains.

Contents

List of Figures

List of Tables

Chapter 1

Introduction

The usage of robots in urban search and rescue missions (USAR) [8] has been gaining a lot of attention since the turn of this century. Several instances of successful application of robots in USAR scenarios have been documented in literature. The Packbot [30] was deployed after the September 11 terrorist attacks, to search for trapped survivors. This was the first prominent application of robots in USAR. It received wide spread media attention and inspired many researchers who were actively working in this direction. The most recent application [12, 11] was during the Fukushima Nuclear Rector Disaster that resulted from a massive earthquake in Japan, in the year 2011. Undeniably, the use of robots would help in curtailing human loss and speed up rescue efforts. These objectives are perfectly aligned to the primary objective of Robotics: to substitute or compliment humans in life endangering scenarios.

1.1 Background and Motivation

Building robots for search and rescue during disaster situations offers many interesting challenges. The robots must be able to traverse through very tight spaces, and move ahead taking minimal support from the unstable surroundings. It is likely that the robot would need to climb step-like(very steep) obstacles which are 1-2 times its body length during exploration. Some interesting mobile robots, such as DIR-2 [16], PAW [27], WHEGS [6], Packbot [30], etc., were developed with enhanced climbing ability. However, their usability in USAR scenarios is limited by their size, as shown in Fig.1.1(a,c,e). Seeking inspiration from nature, it may be noted that small sized and agile robots can perform better in such scenarios. But, the small size puts a limit on maximum propulsive force, and restricts its climbing ability. Keeping these constraints in view, modular robots were proposed as better performers in USAR scenarios [33] .

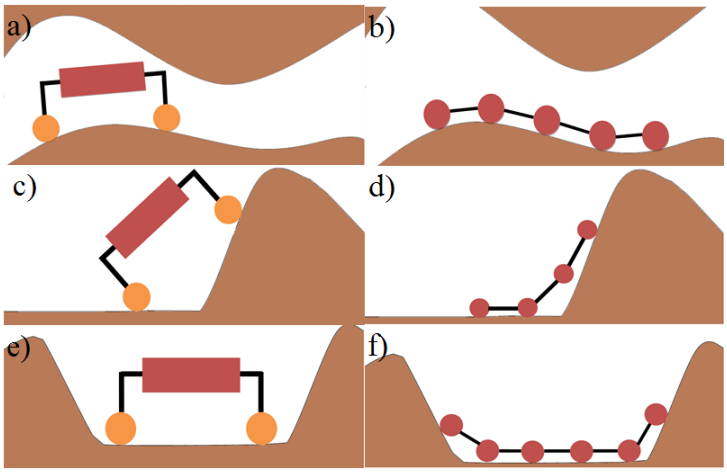

Figure 1.1 Different types of obstacles such as a narrow opening, a big rock and a deep ditch are shown here. A highly redundant robot (b, d and f) can perform better than a conventional mobile robot (a, c and e) in these situations.

Modular Robots offer several advantages, as illustrated in Fig. 1.1. Additionally, in [31] and [34], the author described versatility, reliability and low-cost as the main advantages of such robots. Versatility comes from high degrees-of-freedom. It is more reliable as it can function even if a few modules fail. It is cost effective as it can offer a wide range of climbing and traversing abilities by the mere addition and subtraction of modules, without any major modification. One key disadvantage of modular re-configurable robots is that the individual members have very limited mobility. Alternatively, some researchers have also proposed to develop active/passive linking mechanisms to join multiple off-the-shelf or conventional mobile robots and build a train-like structures to cooperatively solve several rough terrain mobility issues, like climbing steep obstacles. Notable among them are Gunryu [13] , Millibot [7] and [9]. In this work, we address the issues associated with climbing big and steep obstacles for both type of robots mentioned above.

It is worth noting that climbing big step-like obstacles is an important element of any USAR scenarios as it greatly improves the locomotion capabilities of the robot that are discussed in [23]. In [14], these type of highly-redundant robots are additionally termed as snake-like robots. Several types of snake-like robots have been proposed earlier in the literature. They are broadly classified into crawler-type or wheel-type based on the type of locomotion mechanism. They can also be classified based on the mode of actuation used for their locomotion, i.e., active-wheel/active-crawler (AW/AC) and/or active-trunk-joint (AJ). Table 1.1 depicts this classification. Though crawler robots have better climbing ability than wheel robots, the former are slower, bulkier and have low ground clearance. It is also hard to design a water-tight

and dust-proof system for crawler robots [25]. Therefore wheeled robot design is chosen as speed is of vital importance in a rescue scenario.

Table 1.1 Classification of snake-like robots

Existing Robots	Locomotion Mechanism	Trunk Actuation	Robot Category
ACM -R4 [29]	Wheel	Active	AW-AJ
Genbu [17]	Wheel	Passive	AW-PJ
ACM-R3 [14]	Wheel	Active	PW-AJ
Shouryu III,IV,V [2, 3]	Crawler	Active	AC-AJ
Kohga [15]	Crawler	Passive	AC-PJ

The use of active link-joints for step climbing was shown in [32] using a modular robot. However, in [25, 17] the authors have pointed out that the robots using active link-joints are more prone to joint-motor/gear-train damage during traversal when subjected to high reaction forces/moments due to impacts. On the other hand, snake-like robots with passive link-joints are more durable as the joints can freely deform along the terrain. However, they can tip-over while climbing big step-like obstacles or ascending out of ditches. Hence, climbing big step-like obstacles and deep ditches, as shown in Fig. 1.1, is a challenging task. In [25], the authors proposed the use of strings to control the motion of the trunk, and to improve the robot's locomotion capability without any actuators at the trunk-joints. This provides advantages of both active and passive trunk-joints based robots. However, it still requires additional actuators for controlling the strings. The aim of this work is to propose a novel modular robot which can successfully climb big step-like obstacles with minimal slip and ideally no link actuation.

1.2 Proposed Solution

Literature on passive modular robots is less common as it is very challenging to control the internal mobility of highly redundant robots while climbing, without any additional link actuation. The basic robot design consists of three or five modules connected by passive link-joints and active wheels, thus belonging to the AW-PJ (active-wheel passive-trunk-joint) category, as shown in Fig. 1.2.

Initially, a semi-active robot design is developed, where alternate link-joints are actuated. This robot has the natural flexibility offered by the passive systems and some minimal trunk actuation to enforce a control scheme for climbing higher steps. The robot must be able to

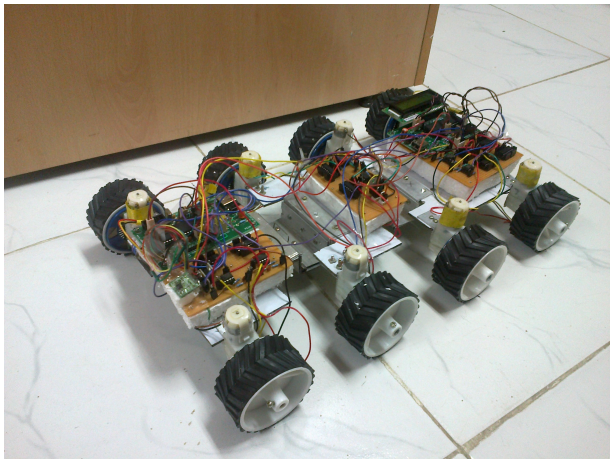

Figure 1.2 A snapshot of the 3-module compliant robot prototype.

climb steps of lower heights using only wheel actuation with the help of passive articulation. The use actuators is limited to climbing bigger steps only.

Later, this design was augmented by replacing motors at the link-joints with passive compliant elements, thus completely eliminating link actuation. In [24], it was shown that the use of springs also helped in absorbing the impact force during collision, and in reducing wheel-slip. However, the climbing ability of the robot was still proportional to its wheel diameter. This limits its usage in urban search and rescue scenarios.

It is also seen that the use of compliant joints improves the climbing efficiency of the robot by maintaining wheel ground contact, and the redistribution of normal forces for generating traction efficiently. The determination of stiffness at the compliant joints is formulated as an optimization problem with an objective to generate minimal spring reaction moments while climbing. This is one of the main contributions of this work. Motivated by the development of this modular robot, a design methodology is also proposed for developing an n- module compliant robot for climbing a given height h on a surface whose coefficient of friction is μ. The successful validation of the methodology in developing a five module robot for climbing a step of 36cm height is also shown.

Terrainability is one of the key performance metrics to asses the performance of a robot designed for outdoor navigation. It is defined as the ability of the robot to tackle rough terrain features without losing stability and forward progress [1]. Note that, the present robot design relies on wheel actuation for its terrain traversal, and it is the only parameter that can be controlled to maintain static equilibrium. However, this is valid only when the wheels are rolling without slipping. So it is very crucial to ensure that slippage is kept low so that the robot can be better controlled. Conventionally, mobile robots used only velocity control, implemented using

wheel encoders, without considering the robot's model. As each wheel's control is indifferent to the overall motion of the robot, this approach lead to considerable slippage.

Wheel-slip could offer considerable resistance to maintain forward motion, and in carrying out wheel odometry. This problem is well studied for SHRIMP([22, 21])and CRAB([26, 19, 18, 28]). It may be noted that the direct application of the formalism shown in these works to a compliant modular robot is not straight forward. In the case of conventional passively articulated robots, the wheels always maintain contact with the ground. Therefore, one set static stability equations are sufficient to describe any arbitrary state of the robot. However, in the case of the compliant modular robot, there will be instances where a wheel pair may leave contact. Hence, different sets of equations are required to reflect the loss of contact. This motivated the development of a formalism that computes the optimal wheel torques required for a compliant modular robot while navigating on uneven terrain. After implementing this controller, there has been a considerable reduction in wheel slip and mean wheel torques across a range of surfaces. This is verified both numerically and experimentally on a wide range of surfaces.

1.3 Research Objectives

- Design modular robots that can climb big step-like obstacles (whose height is atleast two times the robot's individual module length) with minimal or no link actuation.
- To conceive a methodology that determines joint stiffness for an n-module robot to climb an obstacle of an unknown but very big height.
- Minimize wheel-slip in the modular robot to improve its odometric accuracy and energy efficiency.

1.4 Contributions

- A novel model-based controller for climbing big step-like obstacles with a semi-active modular robot.
- Novel compliant link joints that can replace actuated joints without any compromise in the height climbing performance. Additionally, a generalized methodology to design compliant joints for any n-modular robot to climb a given height.

- Development of optimal wheel-torque based controller for a modular robot, to reduce wheel slip.

1.5 Organization of the thesis

In Chapter 1, a general introduction is provided to the all terrain robots and their applications, with a major focus on urban search and rescue. A brief review of the related work is also provided. The modular robot mechanism is detailed in Chapter 2. The control methodologies developed for the semi-active modular robot are described in Chapter 3. The design process for a novel compliant modular robot and its step climbing efficiency are presented in Chapter 4. Extensive simulation results for traversing on unstructured terrain are also illustrated. This is used as a basis to propose a general n-modular robot for climbing any given height. The wheel-torque optimization procedure for wheel-slip reduction and the resulting traction controller design overview are shown in Chapter 5. Subsequently, in Chapter 6 the prototype construction details are given. The compliant robot equipped with the optimal wheel torque based controller is tested on several unstructured terrains, on different kinds of surfaces, and its performance is analyzed. Finally, Chapter 7 outlines the conclusions and future work.

Chapter 2

Design and Static Analysis of a Modular Robot

The proposed robot has 3-modules, each consisting of an independently actuated wheel-pair and a trunk/link. Two adjoining modules are connected using 1 degree-of-freedom (DOF) revolute joints, called link-joints. The wheel- and link-joints are denoted by W_i and J_i, respectively, as shown in Fig. 2.1. The absolute (between module i and ground) and relative (between module i and $i+1$) link joint angles are denoted by θ_i and ϕ_i, respectively.

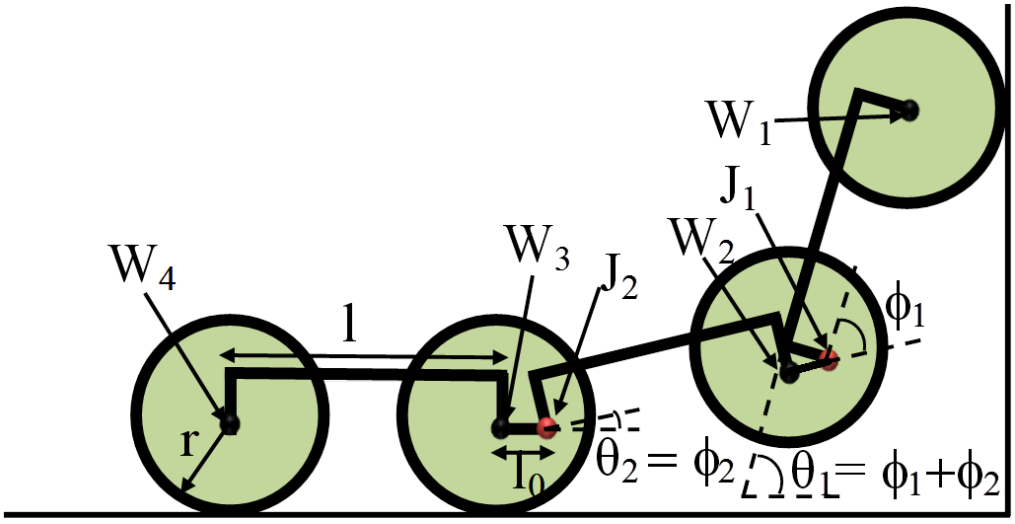

Figure 2.1 The front view of the robot showing the link and wheel joints. The relative angles (ϕ's) and absolute angles (θ's) are also depicted.

Key design considerations of the robot are discussed below:

2.1 Design Considerations

It worth noting that the poor design of modular robots leads to, 1) collision of the link with the ground, while climbing steps or ditches, as shown in Fig. 2.2(a), and 2) inability to naturally ascend the step due resistance caused by the moment due to normal force, as shown in Fig. 2.3(a). The above two criteria are very important in design of the proposed robot and are considered next.

2.1.1 Module Ground Clearance

Providing an appropriate ground clearance can help in avoiding any undesirable collision between the link and obstacles while climbing. Figure 2.2(b) shows the minimum clearance required, denoted as c_{min}, for avoiding collision. It is defined as $c_{min} = c + r$, where $c = l/2 - r\sqrt{2}$, l is length of the module and r is the wheel radius. Note that, the clearance also depends on the shape of the obstacle, and it increases with increase in the sharpness of the obstacle/step. However, the above parameterization holds for step angles $\geq 90^0$ (Fig.2.2(b)).

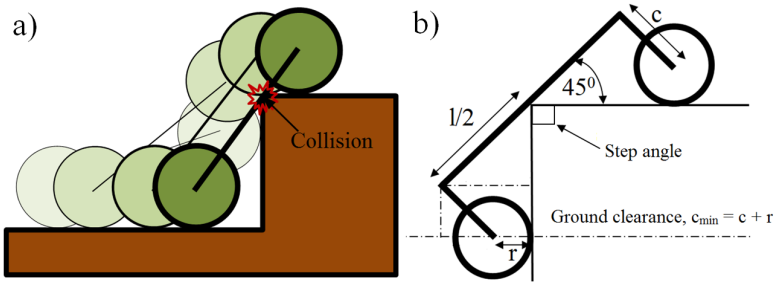

Figure 2.2 Effect of ground clearance: a) An inevitable collision occurs when the module is designed with insufficient ground clearance; b) The minimum ground clearance c_{min} is parametrized in terms of the length of the module(l) and the wheel radius(r).

2.1.2 Link Joint Placement

Selecting the location of the link-joint wisely can improve the climbing efficiency of the robot. Figure 2.3 shows two potential locations for joint placement. In Fig. 2.3(a), the wheel touches the step at a point lower than that of the link-joint. Hence, a clockwise moment will be created due to the normal force developed at the point of contact, causing the robot to fold inwards. This is undesirable, and robot will require external actuation at the link-joint in order to overcome the moment. This can be avoided by lowering the joint to the wheel centers, as

shown in Fig. 2.3(b). The moment thus created at the link-joint acts in the counter clockwise direction, and helps in lifting the module. This ensures natural climbing along the obstacle.

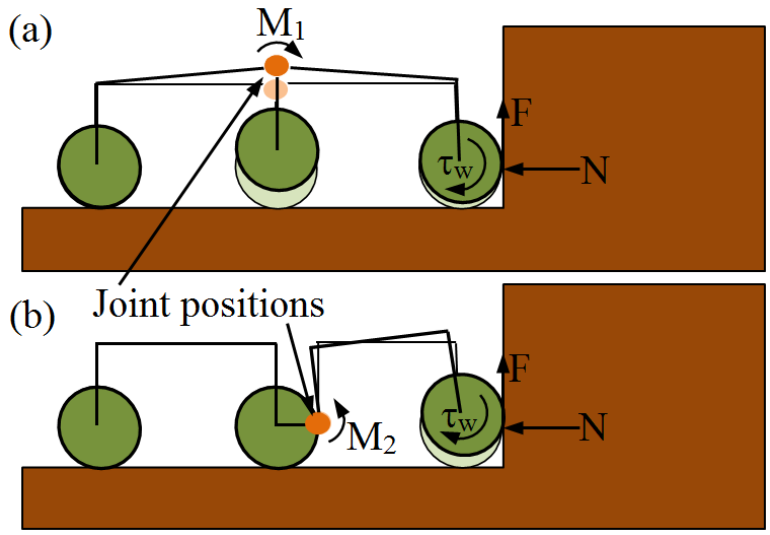

Figure 2.3 Two potential locations for the passive link-joint(PJ): a) Location 1: Clockwise moment (M_1) is created when joint is placed on the top of the module. This moment resists climbing natural climbing motion. b) Location 2: Counter-clockwise moment (M_2) is generated when joint is positioned adjacent to the wheel axis. This naturally aids in climbing.

The robot is wide enough to provide sufficient stability against rolling over. The Specifications of the proposed robot are listed in Table 2.1. Upon finalizing the robot's design, its climbing ability with passive link-joint is analyzed next.

Table 2.1 Specifications of the 3-module robot

Symbols	Quantity	Values(with Units)
l	Link Length	$0.15\ m$
b	Link Breadth	$0.1\ m$
r	Wheel Radius	$0.03\ m$
l_0	Wheel Joint and Link Joint Offset	$0.03\ m$
μ	Coefficient of Friction	0.8
τ_{wmax}	Stall Torque of Wheel Motors	$0.6\ Nm$
m_w	Mass of Each Wheel	$0.1\ Kg$
m_l	Mass of Each Link	$0.3\ Kg$

2.2 Climbing Analysis with Passive link-Joint

Fig. 2.4(a) shows the climbing phase of the robot with passive link-joint. Note that module 1 will continue to climb along the step till it crosses a limiting angle. Beyond the limiting angle, the module will tip-over as shown in Fig. 2.4(b). The moment due to the normal force and self weight will both act in the counter clockwise direction causing the link to tip-over. The limiting angle called tip-over angle (θ_{to}) can be determined based on the position of center-of-mass (COM) of the module as $\theta_{to} = \pi/2 - tan^{-1}(y_{COM}/x_{COM})$, where x_{COM} and y_{COM} denote the COM coordinates of the module. For the proposed robot design, $\theta_{1max} = \phi_{1max} = 72^0$. This tip-over phenomenon limits the climbing ability of the proposed robot, and the robot can only climb obstacles of heights less than or equal to $lsin(\theta_{to})$.

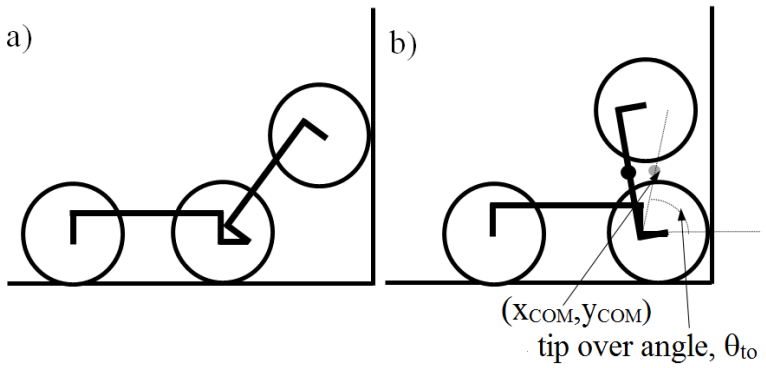

Figure 2.4 Climbing behavior of the passive robot: a) In the climbing phase, it continues to climb the step as long as $\phi_1 \leq \theta_{to}$. b) If the module continues to climb beyond this point, then the moment due to its self-weight changes direction and causes the module to tip over. This phase is called tip over phase.

Alternative methods need to be explored to restrict the links from going past the tip-over angle θ_{to} and subsequently climb bigger steps without tipping over. Ideally, this should be achieved without any major modification to the existing mechanism. The mechanism should be smartly modified to freely allow deformation against smaller angular displacements and constrain it when the angular displacements are larger leading to failure. Spring compliance could be a potential choice provided the stiffness is carefully determined. To determine the optimal stiffness, it is important to first determine the moments generated at the respective link joints when the relative angles(ϕ's) between the links approach tip-over angles(θ_{to}). To obtain the same, a quasi-static model of the robot is developed and the static stability equations are derived to estimate spring stiffness.

This work mainly aims to improve the climbing ability of a passive modular robot. To do the same, we must first estimate the loads acting on the robot due to the environment while

climbing obstacles. This helps in understanding the moment profile at the link joints and that information can be used to design active controllers or passive mechanisms accordingly, to avoid tip-over problem. In the next section, the static model of the robot is derived for this purpose.

2.3 Quasi-Static Model of the Modular Robot

Generally, robots traversing on uneven terrains, do so at relatively lower speeds. Therefore, the dynamics effects are minimal. A static model can give a good approximation of the robot's climbing behavior. In the static model various kind of forces that are acting on the robot, such as friction forces, normal forces, body weight,etc., are taken into consideration. To maintain static equilibrium, the net force in both the $x-$ and $y-$ directions should be equal to zero. The net moment about all the rotating joints (J_1, J_2) should also be equal to zero. The static equilibrium equations of the three-module robot on a general terrain, as shown in Fig. 2.5, are shown below:

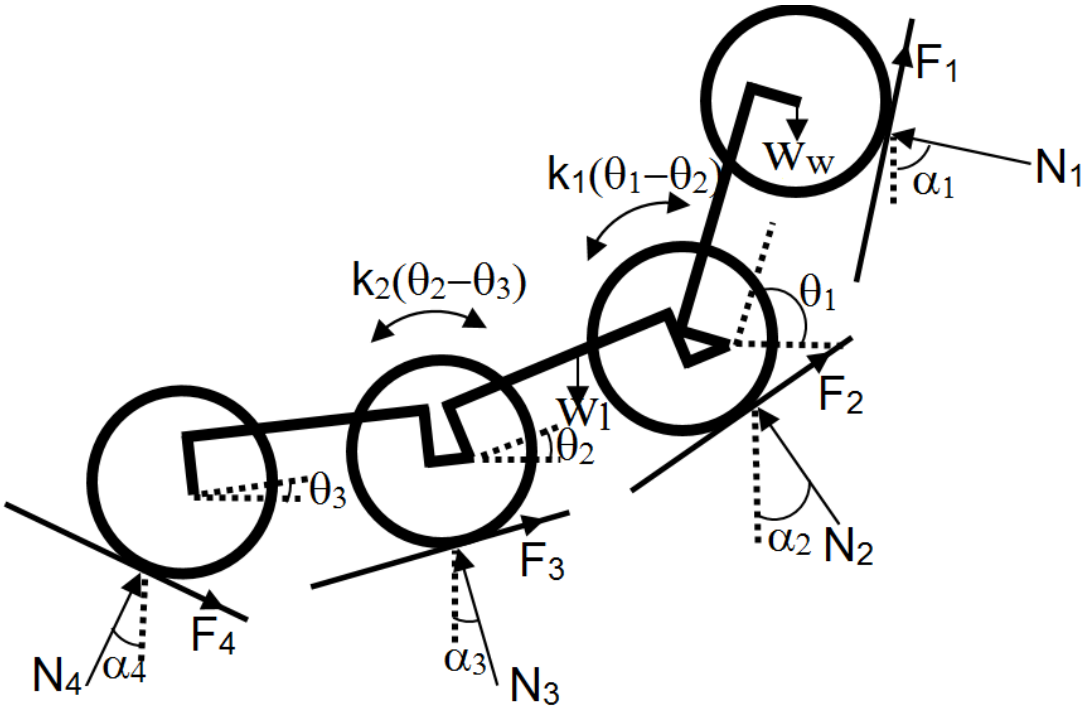

Figure 2.5 The forces and moments acting on the robot for a general terrain

$$\sum F_x = 0 \ :$$

$$\sum_{i=1}^{4} F_i cos\alpha_i - \sum_{i=1}^{4} N_i sin\alpha_i = 0$$

$$\sum F_y = 0 \ :$$

$$\sum_{i=1}^{4} N_i cos\alpha_i - \sum_{i=1}^{4} F_i sin\alpha_i = 3w_l + 8w_w$$

$$\sum M_{J_1} = 0 \ :$$

$$F_1[2l(sin\alpha_1 cos\theta_1 + cos\alpha_1 sin\theta_1) + 2r] + N_1[2l(cos\alpha_1 cos\theta_1 + sin\alpha_1 sin\theta_1)]$$
$$= \tau_1 + w_l[(l/2)cos\theta_1 - csin\theta_1] + 2w_w l cos\theta_1 \tag{2.1}$$

$$\sum M_{J_2} = 0 \ :$$

$$\sum_{i=1}^{2} F_i[2l(cos\alpha_i sin\theta_i + sin\alpha_i cos\theta_i)] + 2F_2 r + \sum_{i=1}^{2} N_i[2l(cos\alpha_i cos\theta_i + sin\alpha_i sin\theta_i)]$$
$$= \tau_2 - \tau_1 + 2w_w l cos\theta_2 + w_l[(l/2)cos\theta_2 - csin\theta_2] + (w_l + 2w_w)(l + l_0)cos\theta_2$$

$$\sum M_{W_4} = 0 \ :$$

$$\sum_{i=3}^{2} F_i[2l(cos\alpha_i sin\theta_i + sin\alpha_i cos\theta_i)] + 2F_3 r + 2F_4 r + \sum_{i=3}^{2} N_i[2l(cos\alpha_i cos\theta_i + sin\alpha_i sin\theta_i)]$$
$$= -\tau_2 + w_l[(l/2)cos\theta_3 - csin\theta_3] + (2w_l + 4w_w)(l + l_0)cos\theta_3 + 2w_w l cos\theta_3$$

It can be seen that there are 5 equations per phase. The first 2 equations ensure the equilibrium of forces in the x and y directions, respectively. The remaining equations denote the moment equilibrium at link-joints J_1 and J_2, and wheel-joint W_3, respectively. In (2.1), $w_w = 2m_w g$ and $w_l = m_l g$ where m_w and m_l denote the masses of the wheel and link, respectively. Moreover, F_i and N_i are the traction and normal forces acting on i^{th} wheel, respectively, and k_i is the spring constant of the spring acting at the i^{th} link-joint. Furthermore, θ_i and α_i denote the absolute link angle and wheel contact angle, respectively. Finally, τ_1 and τ_2 denote the link-joint moments acting at J_1 and J_2, respectively.

In this work we focus on climbing steep obstacles like steps, which are generally harder to climb. Equations for step climbing are obtained in (2.2) by substituting $\alpha_1 = 90^0$ and $\alpha_i = 0, \ \forall i = 2, 3, 4$ in (2.1). Since the robot is symmetric about the sagittal plane, a planar quasi-static analysis of the robot can approximate its real behavior. This, however, is non

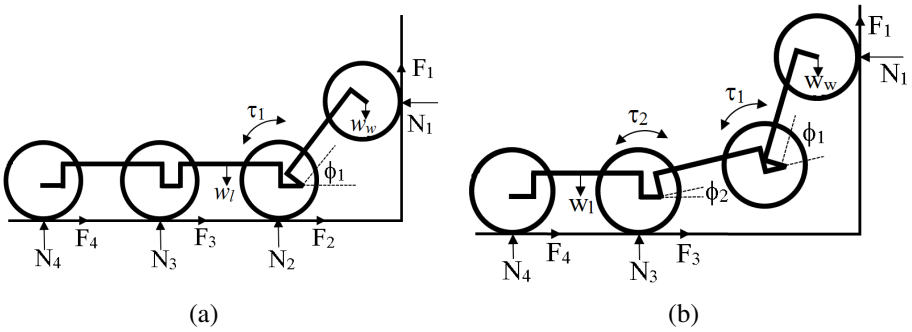

Figure 2.6 The forces and moments acting on the while climbing a step with (a) one climbing link (phase-1) and (b) two climbing links (phase-2), respectively.

trivial for modular robot discussed in this paper. In mobile robots, like, CRAB [20] and PAW [27], the wheels maintain contact with the ground throughout their motion. This enables the formulation of a generalized set of equations for any arbitrary configuration. However, here, the static stability equations change when wheel-pair leaves contact with the ground during the climbing phase of the robot. Therefore, different set of equations have to considered for various configurations of the robot while optimization. In the first phase, the robot climbs heights up to $lsin\theta_{to}$ using only one link, whereas it climbs from $lsin\theta_{to}$ to $2lsin\theta_{to}$ in the next phase with two links. Figs. 2.6(a) and 2.6(b) show the two climbing phases for a 3-module robot. It also depicts the forces and moments acting on it. Equations for Phase-1 and Phase-2 are given in (2.2) and (2.3), respectively, as shown below:

$$
\begin{aligned}
\sum F_x = 0 \quad & N_1 - F_2 - F_3 - F_4 = 0 \\
\sum F_y = 0 \quad & 3w_l + 8w_w - 2F_1 - 2N_2 - 2N_3 - 2N_4 = 0 \\
\sum M_{J_1} = 0 \quad & 2F_1 r + 2F_1 l cos\theta_1 + 2N_1 l sin\theta_1 - \\
& 2w_w l cos\theta_1 - w_l[(l/2)cos\theta_1 - csin\theta_1] \\
& - \tau_1 = 0 \\
\sum M_{J_2} = 0 \quad & 2F_2 r + N_2 l - 2w_w l - w_l(l/2) - \\
& [(2w_w + w_l) - 2F_1](l + l_0) + \tau_1 \\
& - \tau_2 = 0 \\
\sum M_{W_4} = 0 \quad & 2F_3 r + 2F_4 r + 2N_3 l - 2w_w l - w_l(l/2) - \\
& [2(2w_w + w_l) - 2F_1 - 2N_2](l + l_0) \\
& + \tau_2 = 0
\end{aligned}
$$

$$
\begin{aligned}
\sum F_x = 0 \quad & N_1 - F_3 - F_4 = 0 \\
\sum F_y = 0 \quad & 3w_l + 8w_w - 2F_1 - 2N_3 - 2N_4 = 0 \\
\sum M_{J_1} = 0 \quad & 2F_1 r + (2F_1 - 2w_w) l cos\theta_1 \\
& - w_l[(l/2)cos\theta_1 - csin\theta_1] \\
& + 2N_1 l sin\theta_1 - \tau_1 = 0 \\
\sum M_{J_2} = 0 \quad & 2w_w(l + l_0)cos\theta_2 - w_l[(l/2)cos\theta_2 - csin\theta_2] \\
& - [(2w_w + w_l) - 2F_1](l + l_0)cos\theta 2 \\
& + 2N_1(l + l_0)sin\theta_2 + \tau_1 - \tau_2 = 0 \\
\sum M_{W_4} = 0 \quad & 2F_3 r + 2F_4 r + 2N_3 l - 2w_w l - w_l(l/2) - \\
& [2(2w_w + w_l) - 2F_1 - 2N_2](l + l_0) + \tau_2 = 0
\end{aligned}
$$

For Phase-1, $\phi_1 = \theta_1 = sin^{-1}(h/l)$ and $\phi_2 = 0$, and for Phase-2, $\phi_2 = \theta_2 = sin^{-1}(h - lsin\theta to)/l)$ and $\phi_1 = \theta_{to} - \phi_2$. Here, the second module will begin to climb only after the first module reaches $lsin\theta_{to}$. In Phase-2, ϕ_1 is designed such that if ϕ_2 increases ϕ_1 decreases by the same amount maintaining $\theta_1 = \theta_{to}$, in order to avoid tipping over. This analysis is utilized in the subsequent chapters while formulating an optimization problem to estimate the optimal compliance desired in link-joints.

2.4 Conclusions

In this chapter, the modular robot model is introduced. The key design choices such as minimum ground clearance and link joint location are discussed in detail. The step climbing motion of the robot is analyzed and the tip-over problem is identified. As a first step to address this problem, the static equilibrium equations for step climbing are derived. This static analysis will be utilized in the subsequent chapters to develop model-based controllers or compliant link-joints for climbing big step-like obstacles without tipping over.

Chapter 3

Step Climbing using a Semi-Active Robot

3.1 Introduction

In the previous chapter, the tip-over problem in passive modular robots was discussed. Some active or passive mechanism needs to be conceived to restrict the link modules from tipping over while climbing big step-like obstacles. Actuators can be used at every link joint and the configuration of the robot can be controlled while climbing steps. Though this is the most practical solution and widely used, it has some disadvantages which were briefly discussed in Chapter 1. It is desirable that the robots made for USAR missions are low-cost and robust to impacts. Additionally, they need to be very light-weight to ensure that they don't add load onto semi-collapsed structures while traversing on them. Motors are generally heavier and having too many motors adds weight to the robot. Secondly, motors gear-trains are most susceptible to damage during impacts.

Keeping these issues in view, the primary objective of the new semi-active robot design is to use least number of link actuators to climb higher and avoid tip over. Initially, only link joint J_2 is actuated. Link joint J_1 is left passive to allow the robot to naturally deform along obstacles. When the obstacle, is big enough to cause tip-over, the motor at J_2 is actuated to reduce joint angle ϕ_1 and maintain it under θ_{to}. Upon implementing this control law, it was seen that the torque generated by the motor at J_2 caused a reaction moment on module-3 causing wheel-pair-4 to lift off the ground. This is undesirable as the torque required to lift module-2 is being spent in lifting module-3 as well. To mitigate this problem, an additional motor is fitted at link-joint J_4 to balance and suppress the reaction moment caused due to the motor at J_2. The final robot model with two actuators at link-joints J_2 and J_4, respectively, is shown in Fig. 3.1. The control strategies used at each of these joints is discusses in the next section. With

this new design, the robot is shown to climb heights upto twice it's link length without tipping over.

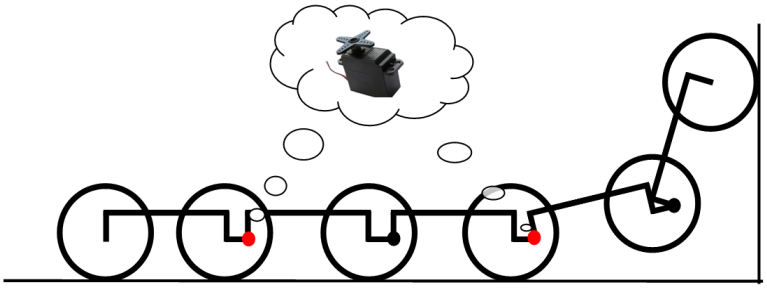

Figure 3.1 An image of the robot indicating the link-joints that are actuated on this semi-active design

The control algorithm is designed to maintain $\theta < \theta_{to}$ throughout the ascent. Here, θ_i is defined as the angle between the i^{th} link and the ground. The angle θ_i can also be defined in terms of relative joint angle ϕ_i (between links i and $i+1$) as,

$$\theta_i = \sum_{i}^{n} \phi_i \tag{3.1}$$

Noting that the mechanism shown in figure fails when $\theta \geq \theta_{to}$, it can be deduced that a control over the relative joint angles ϕ_i between the links can help in climbing greater heights before θ_1 approaches θ_{to}.

3.2 Control Strategy I

This strategy deals with the control of the joint at J_2, for maintaining vehicle stability. When only link 1 is climbing the step and link joint J_2 is actuated, two effects are seen, 1) link-1 is lifted up and 2) ϕ_1 is reduced. Therefore, the robot is able to climb higher steps, which could not have been possible with passive joints. To implement this control algorithm on the vehicle, a control law is developed. It is worth noting when $\phi_1 << \theta_{to}$, the robot can climb without any actuation at the link joints. Thus, energy is conserved by minimizing the actuation of joint J_2 by setting up a threshold value. Hence, we define $\phi_c = \theta_{to} - 15^0$, the threshold angle, below which the robot works as a passive mechanism.

For the system under study, $\theta_{to} = 72^0$ and hence $\phi_c = 58^0$. Let an error e_i be defined for the i^{th} joint angle as

$$e_i = \phi_i - \phi_c \tag{3.2}$$

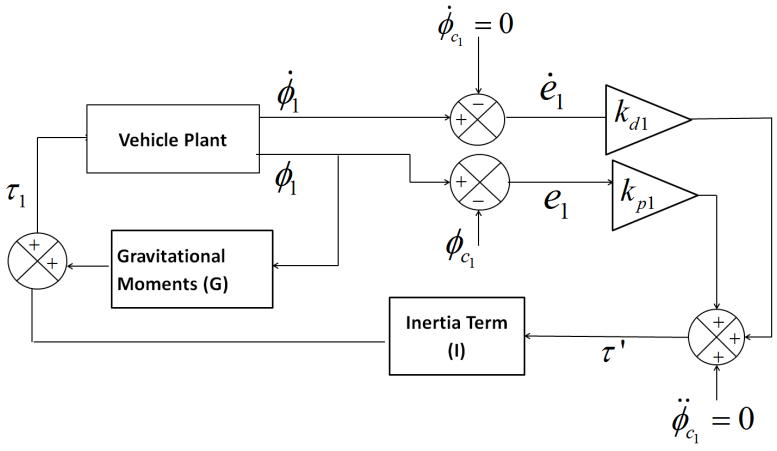

Figure 3.2 Model Based Control for controlling Link-1

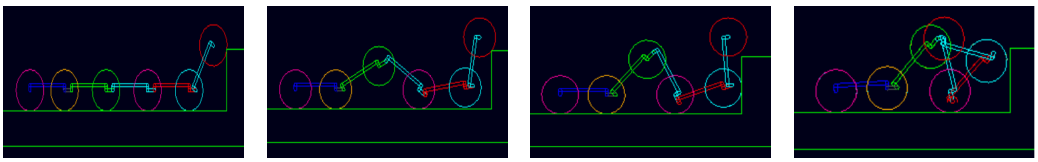

(a) (b) (c) (d)

Figure 3.3 Snapshots of a system failing to climb a step of 180 mm using only Strategy I

With the above definition, a control system is designed the block diagram of which is shown in Fig. 3.2.

When the error obtained from (3.2) is greater than zero, the actuator at J_2 is activated. The torque actuation of the motors can be written as

$$\tau_1 = \alpha\tau_1' + \beta \tag{3.3}$$

$$\tau_1' = \ddot{\phi_{c1}} + k_{p1}e_1 + k_{d1}\dot{e_1} \tag{3.4}$$

In (3.4), k_{p1} and k_{d1} are proportional and derivative gains of the control system. In (3.3), α is the inertia of links-1 and -2 about joint J_2. β balances the moments generated due to gravity.

It is worth noting that when robot starts climbing, its 1^{st} and 2^{nd} links lift up in the beginning. The model based control of those two links is carried out by assuming them to be a 2-link robotic system. Other links are not controlled as they assumed to be on the ground.

The simulation results are shown in Figs. 3.3(a)-3.3(d). As stated earlier, motors are actuated to control joint angles between the links only when a certain threshold (ϕ_c) is breached. Figure 3.3(c) depicts that as the second wheel is being lifted, the reaction moment generated

lifts link-3 off the ground. As both links-3 and -2 were being lifted, the angular displacement of link-2 with respect to the ground (i.e., θ_2) was insufficient for successful climbing motion. As a result the mechanism failed to climb the step. To address this issue, a new control strategy is proposed, as described in the next section.

3.3 Control Strategy II

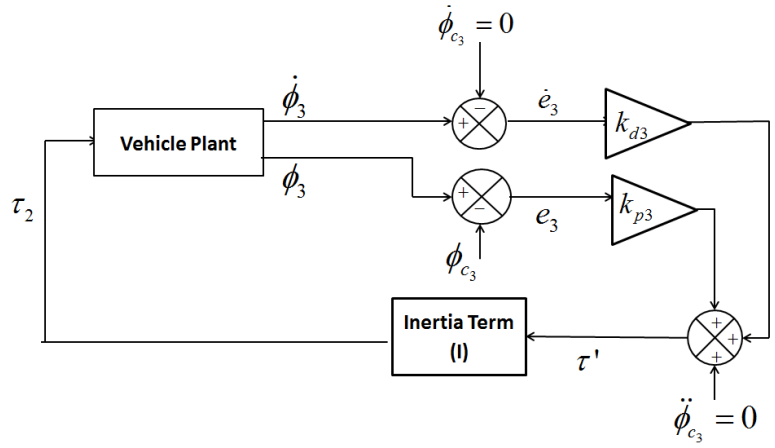

Figure 3.4 PD Control for countering the reactive moment

This strategy uses two active joints at J_2 and J_4 for maintaining stability while climbing steps. Here, joint J_2 is controlled using strategy illustrated in the previous section while joint J_4 is controlled using a new PD control law. It is necessary to balance the reaction moment generated while actuating joint J_2 as detailed in Control Strategy-I. In this strategy, an extra motor is used at link joint J_4 for this purpose. A PD control scheme is used to counter the reactive moment acting on link-3 . This is actuated only when $\phi_3 < 0$ and joint J_2 is active. The PD control law ensures that active joint J_2 only lifts link-2 while it keeps link-3 grounded. The control architecture for the same is shown in the Fig. 3.4

It is worth noting that the actuation of J_4 might lift off the fifth wheel when the reaction moment to be balanced is high. In order to overcome this disadvantage, a torsional spring is fitted at the passive joint $L3$. One cannot choose a spring of high stiffness as this makes the joint stiff. this may limit the climbing ability of the vehicle. After carefully considering the above aspects, a torsional spring of stiffness 2 Nm/rad is chosen. Figs. 3.5(a)-3.5(f) show that the mechanism was successfully able to climb a step of height 330 mm using the proposed strategy.

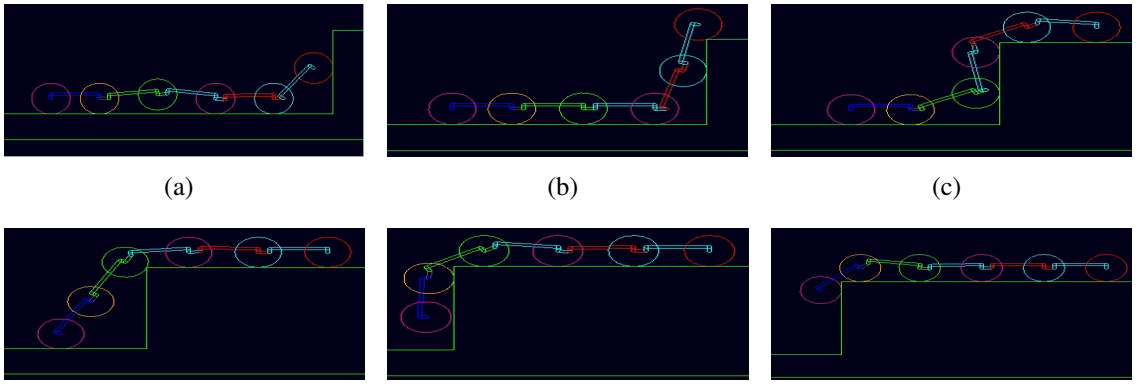

(a) (b) (c)

(d) (e) (f)

Figure 3.5 Snapshots of the robot climbing a step of height 330mm using Control Strategy II

3.4 Results

The robot was simulated in the MSC ADAMS software's dynamics simulation environment to study its performance on steps of varying heights. The Step height was parametrized in terms of link length. The speed of the robot is $18\ cm/s$. The values of k_{p1} and k_{d1} for the model based control in (3.4) are taken as 20 and 4, respectively. Similarly, values of k_{p2} and k_{d2} used in the PD control at link joint J_4 are 80 and 10, respectively.

Fig. 12(b) shows the amount of torque required at the motors during ascent. It can be seen that, while ascending the first step, J_4 applies nearly equal amount of torque(in the counter direction) as J_2. Fig. 12(a) shows the plot of e_1 with respect to time, calculated after the angle ϕ_1 reaches threshold angle, $\phi_c = 45^0$. The threshold is lowered to study the performance of the controller at a lower threshold value. The Control Strategy succeeded in ensuring that link 1 doesn't tip over during its ascent. Thus, the robot achieves the desired climbing motion for heights upto $330\ mm$ which is nearly 1.8 times its link length.

Simulations were also carried out on irregular terrains, as shown in Figs. 3.6(d)-3.6(j). The modularity and passivity of the robot give it a natural edge while traversing an irregular terrain. The body of the robot is able to deform itself along the shape of the obstacle and in areas where the angle of deformation is greater than ϕ_c, the active joint helps it in climbing without tipping over.

3.5 Conclusions

Two control strategies have been presented to achieve step climbing here. In the first strategy only joint J_2 was actuated when $\theta_1 \geq \theta_c$. This strategy showed some improvement over the

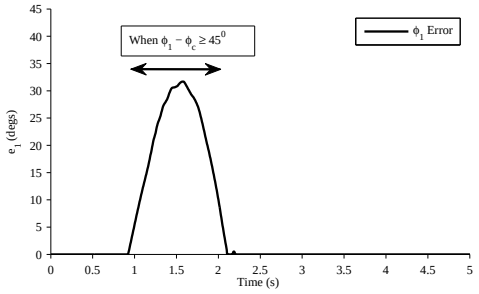

(a) Error vs Time plot

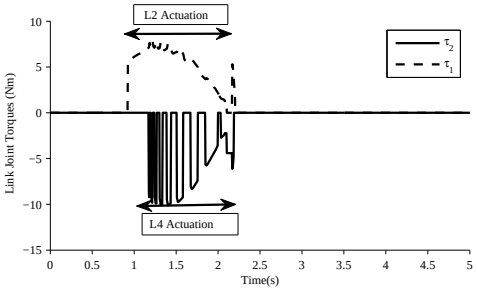

(b) Active joint torques vs Time

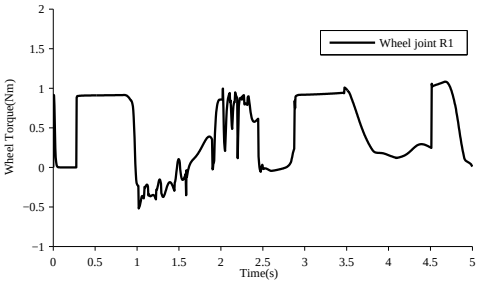

(c) Wheel torques vs Time

passive mechanism but it failed to climb heights higher than 1.2 times the link length. In the second strategy joints J_2 and J_4 have been actuated to overcome the above disadvantage. The robot was successfully able to climb the height equal to 1.8 times the link length. The novelty of this robot lies in the use of passive articulation to traverse over smaller steps and link actuation only for climbing bigger steps. This makes this robot very desirable for traversing on an irregular terrains and step-like obstacles in an energy efficient manner. However, the robot's climbing ability is limited to heights less than $2lsin\theta_{to}$, which is equal to 1.8 times the link length in this case. To climb even bigger obstacles, additional link actuation may be needed. The additional actuators also need to have high torque rating. Therefore, this design cannot be extended for many modules.

Alternatively, a compliant modular design is proposed in the next section. The link actuators used for controlling robot configuration are replaced by torsional springs. This not only makes the robot lighter and more durable. The compliant joints are designed to resist tip-over while allowing the robot to passively articulate along smaller obstacles. In [24], it was also shown that the use of springs also helped in absorbing the impact force during collision, and in reducing wheel-slip. The design methodology for this compliant robot is described in the next chapter.

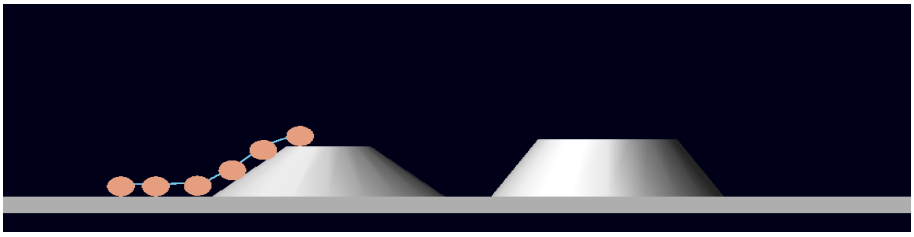

(d)

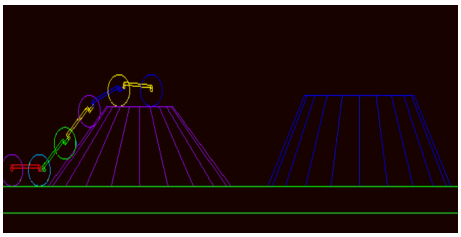

(e)

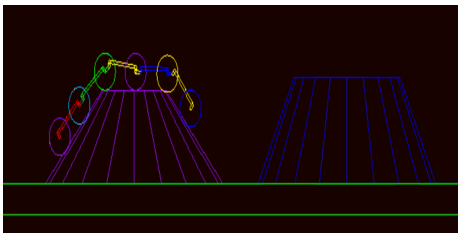

(f)

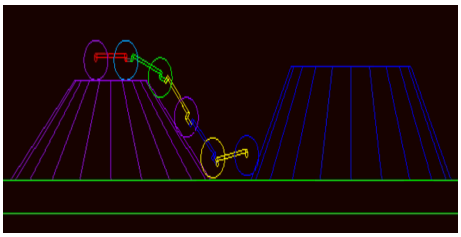

(g)

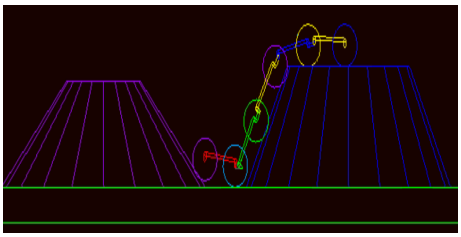

(h)

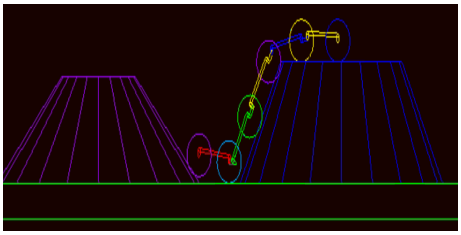

(i)

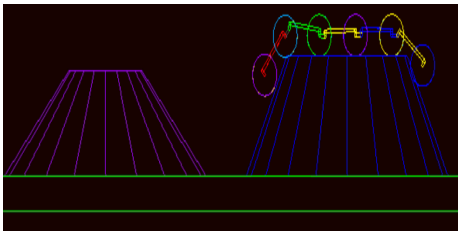

(j)

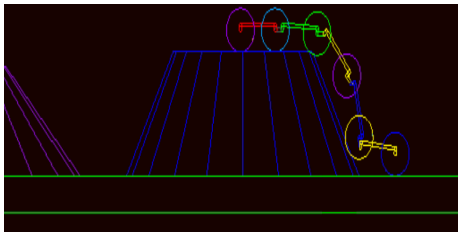

(k)

Figure 3.6 Snapshots of the robot climbing steep obstacles

Chapter 4

Step Climbing using a Passive Compliant Robot

4.1 Introduction

In the previous chapter, a semi-active modular robot was proposed to climb big step-like obstacles. It climbing ability limitations were noted and it was desired to develop modular robots whose climbing ability could be enhanced by adding more modules without increasing the average weight per module. As the obstacle height increases, higher torque motors would be needed at the link joints and more batteries need to be stacked to power them. This increases the module weight exponentially.

An alternative solution is proposed for posture control which completely eliminates the use of motors. The passive link joints J_1 and J_2 are equipped with springs that can generate sufficient reaction moment at the joints to avoid tip-over. An illustration of the new compliant robot design is shown in Fig. 4.1.

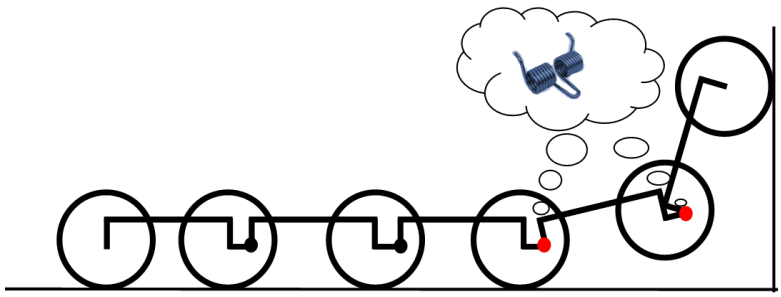

Figure 4.1 An image of the robot indicating the link-joints equipped with springs in the compliant design

Spring elements are generally extremely lightweight and do not require any additional energy. Secondly, springs have are ideal to temporarily store energy and release it for propelling

the robot, when required. For example, when a robot collides with the step, springs store the linear momentum generated in the x-direction and release it to propel in robot in the y-direction. This greatly improves energy efficiency and also minimizes loss of energy during impact. However, estimation of spring stiffness is a non-trivial problem. A stiff spring reduces the natural flexibility offered by passive joints. On the other hand, a pliant joint may not resist the modules from tipping over. This problem of stiffness estimation is discussed in sufficient detail in the following section:

4.2 Compliant Joint Design

The stiffness of a compliant joint plays a key role in the overall performance of the robot. For the robot shown in Fig. 2.1, designing J_1 with high stiffness causes the wheel-pair at W_2 to lift off the ground early. This results into reduction in the push force required for climbing. On the other hand, use of joint with low stiffness at J_1 may not be able to resist moment causing tip over. Therefore, an optimal value for stiffness has to be determined such that the wheel-pair lift off the ground as late as possible, and tip over is avoided. Therefore, stiffness estimation is formulated as an optimization problem with the objective to minimize moments at the joints J_1 and J_2 while climbing. Note that the dynamical effects are neglected as the robot moves with low velocities during climbing phase.

4.2.1 Optimization Formulation

Tip over can be avoided if the moments generated by springs can balance the net moment generated at the joints. For this, climbing maneuver from $h = 0$ to $2lsin\theta_{to}$ is discretized into p set points, and the moment profiles for joints J_1 and J_2 are obtained using the static stability equations. It may be noted that, the traction and normal forces, at the wheel-ground interface, appearing in the static stability equations are difficult to determine accurately without direct sensing. Therefore in the numerical model, they are generally assumed to be unknowns and the static stability equations are under-determined [27]. Though, a least norm solution can be obtained, it may not be of physical significance. Hence, calculation of moments at the joints, and traction and normal forces are formulated as an optimization problem. The objective function for the optimization is taken as minimization of the joint moments.Note that, a direct minimization of link-joint moments might lead to a very non-linear and unrealistic stiffness profile. Therefore, the objective function is altered to minimize the link-joint moments between

successive set-points. It is given below:

$$\begin{aligned} \underset{\mathbf{D}}{\text{minimize}} \quad & \sum_{j=1}^{p} (\boldsymbol{\tau}_j - \boldsymbol{\tau}_{j-i})^2 \\ \text{subject to} \quad & \mathbf{F} \leq \mu \mathbf{N} \end{aligned} \tag{4.1}$$

where, $\boldsymbol{\tau} = [\tau_1 \ \tau_2]^T$, $\mathbf{F} = [F_1 \ F_2 \ F_3 \ F_4]^T$, $\mathbf{N} = [N_1 \ N_2 \ N_3 \ N_4]^T$, and the vector of design variable $\mathbf{D} = [\mathbf{F}^T \ \mathbf{N}^T \ \boldsymbol{\tau}^T]^T$. Moreover, F_i's and N_i's denote traction and normal forces acting at wheel-pair i, and τ_i's denote the moments at the link joints. Note that the traction forces are constrained by the maximum torque (τ_{wmax}) of the wheel motors as $F \leq \tau_{wmax}/r$. The system is also constrained by the static stability equations of the robot, which are derived in the next subsection.

4.2.2 Quasi Static Model for the Compliant Robot

Since the robot is symmetric about the sagittal plane, a planar quasi-static analysis of the robot can approximate its real behavior. This, however, is non trivial for multi-module robot discussed in this paper. In mobile robots, like, CRAB [20] and PAW [27], the wheels maintain contact with the ground throughout their motion. This enables the formulation of a generalized set of equations for any arbitrary configuration. However, here, the static stability equations change when wheel-pair leaves contact with the ground during the climbing phase of the robot. Therefore, different set of equations have to considered for various configurations of the robot while optimization. In the first phase, the robot climbs heights up to $lsin\theta_{to}$ using only one link, whereas it climbs from $lsin\theta_{to}$ to $2lsin\theta_{to}$ in the next phase with two links. The static model of the robot used for this analysis is already described in Section 2.3, Chapter 2.

4.2.3 Estimation of stiffness

The profile of joint moments ($\boldsymbol{\tau}$) versus joint angles ($\boldsymbol{\phi} = [\phi_1 \ \ \phi_2]^T$) obtained from the above optimization is shown in Fig. 4.2 with a solid curve. The profile is slightly non-linear as evident from the figure. Hence, a least squares approximation is carried out as

$$\underset{\mathbf{k}}{\text{minimize}} \quad \sum_{j=1}^{p} (\boldsymbol{\tau}^j - \mathbf{k}\boldsymbol{\phi}^j)^2 \quad , \tag{4.2}$$

where $\mathbf{k} = diag(k_1, k_2)$ and k is the stiffness of the i^{th} joint. The least squares fit for both the joints is also shown in Fig. 4.2 by dotted lines.

Generally, torsional springs are unidirectional in nature. Therefore the spring that can resist counter clockwise moments at J_1 during positive angular displacements, cannot apply resisting clockwise moments when there is a negative angular displacement. Therefore, two springs will be used instead. Accordingly, the static analysis is also decoupled. Note that, τ_1 and τ_2 will always act in such a way that they balance the net moments at J_1 and J_2, respectively. The torsional springs that resist tip-over while climbing up are compressible springs which only act when there is a positive displacement of angle ϕ_1. Therefore, an additional spring needs to be added to the robot such that it only acts for negative displacements of ϕ_1, thus avoiding the undesirable folding configuration occurring during descent.

According to the results obtained from the above optimization procedure, a compliant joint was developed at J_1.Values of k_1 is determined as $0.0105N - m/deg$ while k_2 is of order 10^{-6}, and hence, it is assumed to be zero. It is also desired that the springs only act against counter-clockwise moments and don't resist any clockwise moments. This helps in freely deforming on an uneven terrain without any resistance when there is no scope for tipping over. Hence, the spring is fitted to module 2 and it only touches module 1 without any permanent connection. This enables the springs to act only when there is a positive angular displacement between the two modules.

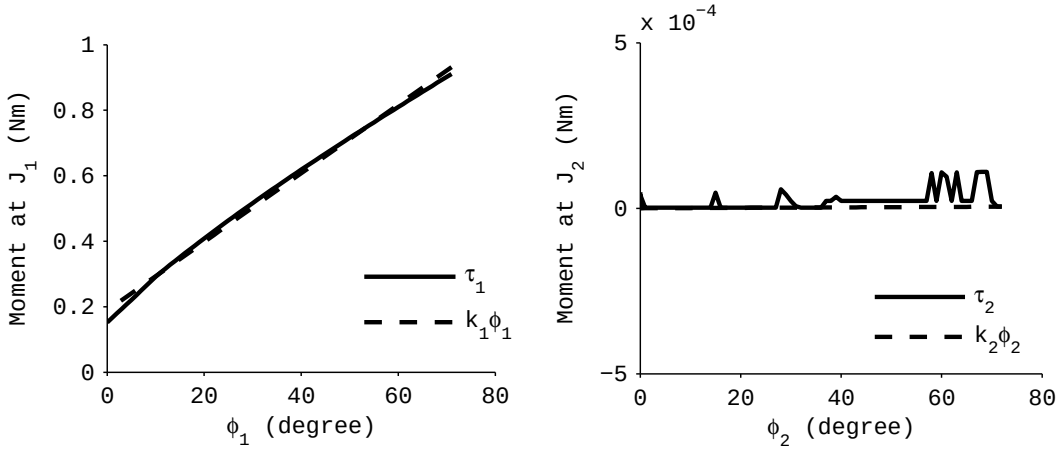

Figure 4.2 Moment plots for joints J_1 and J_2: The plot shows the desired moments obtained from the optimization procedure (solid line) and the moments generated by the optimal spring (dotted line). The slope of the the dotted line yields the spring stiffness value

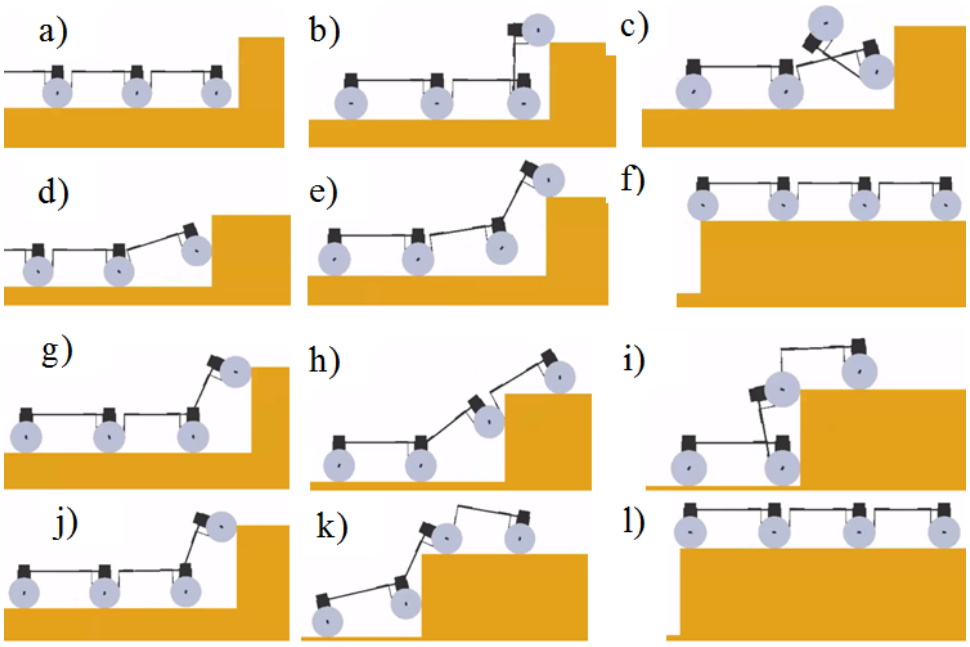

Figure 4.3 Step climbing ability of the 3-module robot: a)-c) Case-1: the passive robot tips over while climbing a height of 14 cm; d)-f) Case-1: it successfully climbs the step of 14 cm using a compliant joint at J_1; Case-3: g)-i) the robot with a compliant joint at J_1 manages to climb a height of 16 cm but is unable to pull the remaining links; Case-4: j)-l) it is able to fully climb a height of 16 cm using compliant joints at J_1 and J_2

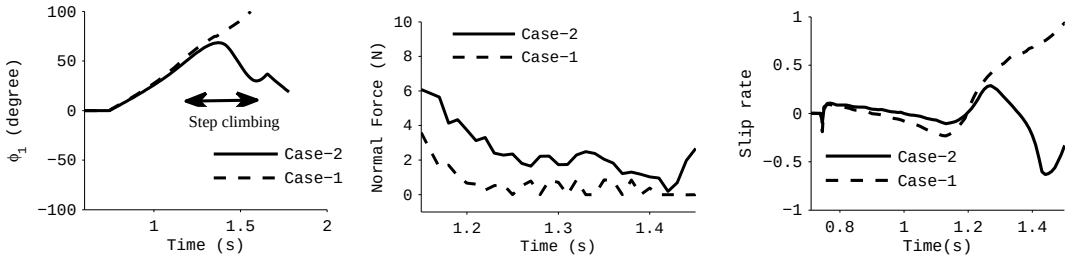

Figure 4.4 Plots to analyze robot's climbing behavior while climbing a 14cm step: a)-c) The comparison of the joint angle (ϕ_1), normal force(N_1) and slip rate(at Wheel 1) between cases with spring (Case-2) and without spring (Case-1) at J_1

4.3 Design Validation

Four different step climbing experiments were carried out to show the efficacy of the compliant joints in improving the climbing ability of a the robot. Each row in Fig. 4.3 shows the snapshots of a different experiment. In Case-1 (Fig. 4.3(a)-(c)), the robot consisting of joints without springs failed to climb a step of height 14cm. On the other hand, the same robot (Case-2), with a spring at J_1, was able to successfully climb over the step, as shown in Fig.

4.3(d)-(f). Figure 4.4(a) shows the plot of joint angles ϕ_1 for the above two cases. In Case-1, the absolute angle increased indefinitely and resulted in tip over, whereas in the second case the angle rose till $68^0(\approx \theta_{to})$ and then decreased as it successfully climbed the step. The use of compliant joint in Case-2 increased the normal force, N_1, at wheel-1 facilitating the wheels to apply more traction (F_1) and thus successfully climbed without slipping, as shown in Fig. 4.4(b). Interestingly, in Case-1 wheel-1 lost contact with the wall multiple times. This is due to the fact that the normal force became zero several times, as shown in Fig. 4.4(b). While in Case-2, the wheel never lost contact with the step, i.e., $N_1 > 0$. This advantage confirms the superiority of the compliant joint over mechanical lock. Additionally, the slip rate was found to be more bounded in Case-2 than that of Case-1 as depicted in Fig. 4.4(c).

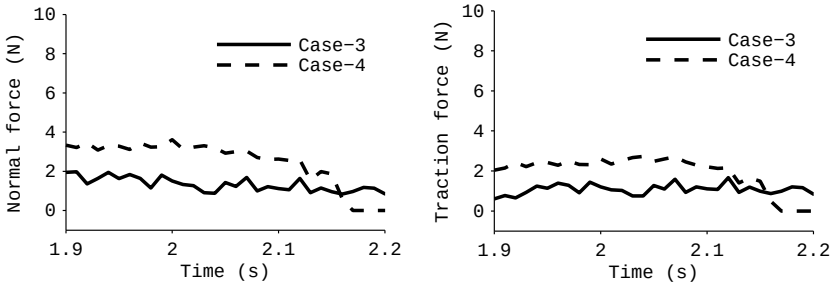

Figure 4.5 Utility of spring at J_2 while climbing a step of 16cm: Plots showing the variation Normal and Traction forces at wheel 2 with spring (Case-4) and without spring(Case-3) at J_2.

In Case-3 (Figs. 4.3(g)-(i)), the robot with only compliant joint at J_1 was made to climb a step of height 16 cm. The robot was able to climb height of 16 cm against the wall but failed to pull up the remaining modules due to the lack of push force as illustrated in Fig. 4.3(i). Note that the optimization only takes into consideration the climbing phase of the robot, hence, it may happen that the robot may climb height h but not have enough pulling force to lift remaining modules. In other words, the traction force F_2 reaches the limiting case μN_2 thus not allowing the wheel to apply greater traction to climb the step, as depicted in Fig. 4.5 with solid lines. However, this limitation can be overcome using another compliant joint at J_2 having the same stiffness value as that of J_1. In case-4 (Figs. 4.3(j)-(l)), the robot with two compliant joints successfully climbed a step of 16cm height. Here, the normal force at wheel-2 increased, and this allowed it to apply greater traction force, as shown in Fig. 4.5 with dotted lines.

To further confirm these results across different heights, additional numerical studies were carried out for heights 15 and 17 cm. The traction and normal force plots for wheels 2,3 and 4 at heights between $14 - 17$ cm are shown in Figs. 4.6 and 4.7, respectively. From these plots, it can be seen that the normal force at wheel 2 decreases due to compliance while the respective

normal forces at wheels 3 and 4 increase. This results in the traction force also following the same trend. Since the normal force is getting redistributed between wheels 3 and 1, the traction force at these wheel increases enabling the robot to successfully climb the big obstacle.

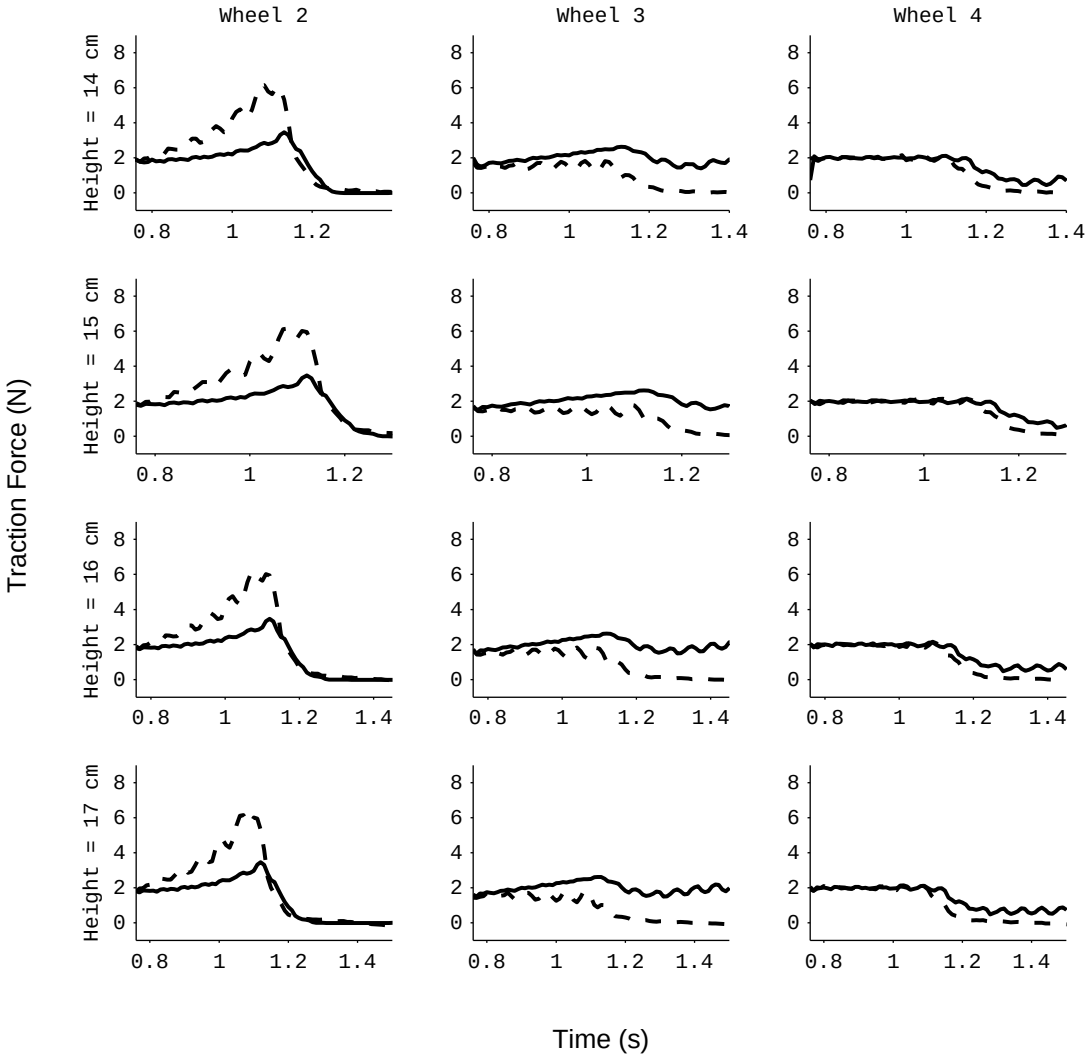

Figure 4.6 Traction force plots with springs(solid line) and without springs(dotted line) for wheels 2-4 at heights between 14-17 cm

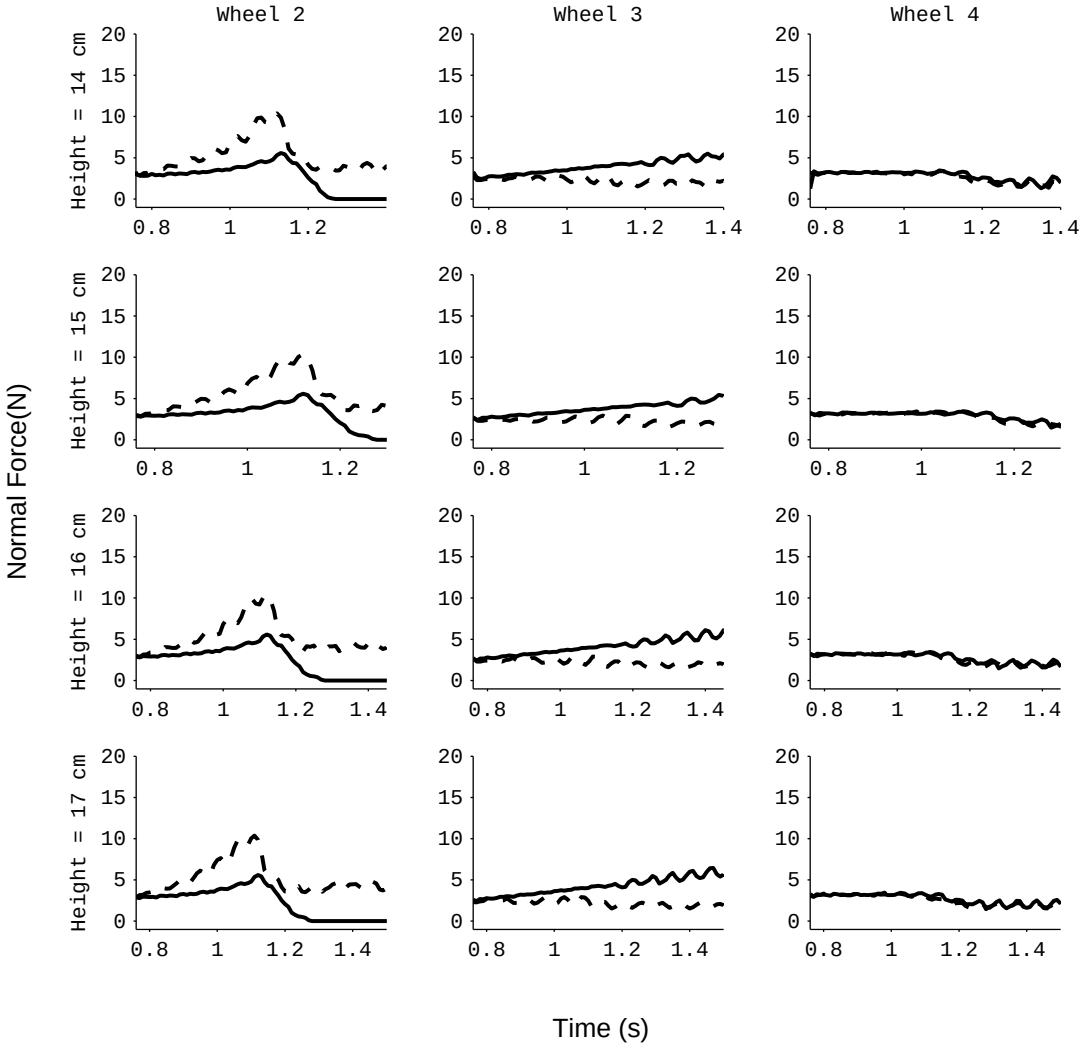

Figure 4.7 Normal force plots with springs(solid line) and without springs(dotted line) for wheels 2-4 at heights between 14-17 cm

In addition to structured obstacles, the robot's traversing ability was also tested and successfully verified on an unstructured terrain, as shown in Fig. 4.8. In the next section, this compliant joint design procedure is extended to an n modular robot to climb a step of any given height.

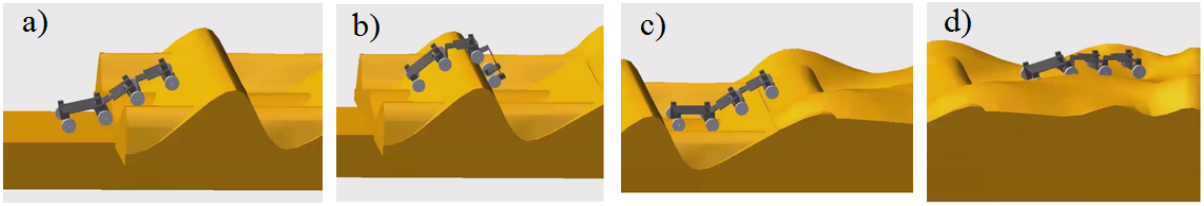

Figure 4.8 The 3-module compliant robot traversing on a highly uneven terrain

4.4 Height Climbing Ability of an n-module Compliant Robot

A general methodology has been developed for estimating the maximum height climbing ability of an n-module compliant robot. This height climbing ability depends chiefly on the coefficient of friction μ and the maximum wheel torque τ_{wmax}. For a practical modular robot design, the quasi-static analysis based optimization formulation can be used to determine the maximum height, h_{max}. To this end, firstly, a trajectory for tip-over-free step climbing is generated for some large height value. It is then discretized into p set-points and the joint angles ϕ_i for all the set-points are derived. They are then used to obtain the static stability equations. Note that, an n-module robot has $n+1$ wheel-pairs and during the climbing maneuver, one-by-one, n wheel-pairs may lift off the ground to successfully climb without tipping over. As each wheel-pair lifts off the ground, the static-stability equations for the system change. To reflect the same, the climbing process of the robot is divided in to n phases, where each phase uses one set of static stability equations. Phase transition occurs from Phase-i to Phase-(i+1) when $\theta_i \approx \theta_{to},\ \forall i \in n$. This implies that a phase transition occurs after every $lsin\theta_{to}$ increase in height. The optimization problem is carried out for all the p set points with the stability constraints changing after every phase.While evaluating the optimization procedure for all the set points, it can be noted that, at a certain set point, i.e., at a certain desired configuration of the robot, the static-stability equations are violated or a steep increase in moment values, τ_i, is noticed. The preceding set point is the height h_{max} that an n-modular robot can successfully climb. The detailed procedures for obtaining joint trajectories and static stability equations, are discussed in the following sub-sections.

4.4.1 Determination of the Joint Trajectories

Designing the joint trajectories for an n-module robot can be a challenging task. For this, a trajectory is developed first for the COM of the first wheel-pair and the corresponding joint motions are derived next. Trajectory of the first wheel-pair ideally follows the profile of a step or obstacle. For climbing the step, as shown in Fig. 4.3, trajectory of the first wheel can be

assumed to be a straight line of a large length value. Next, the trajectory is discretized into p set-points and the desired joints angles (ϕ_i's) are then determined at each set-point. It is ensured that the absolute angles θ_i's of all the climbing links lie under θ_{to}, to avoid tip over. This can be achieved by progressively increasing the relative angle (ϕ_{i+1}) at the succeeding joint and decreasing that of the preceding joint (ϕ_i), as the height keeps on increasing. This is the key idea used for climbing any height h using an n-module compliant robot without tipping over. The joint angles ϕ_i for different set-points can be obtained by solving the set of equations given in (4.3).

$$h = \sum_{i=1}^{n} lsin\theta_i \quad where, \quad \theta_i = \sum_{i=1}^{n} \phi_i \quad \forall i \in n \tag{4.3}$$

The procedure for solving the above equations for Phases-1 and -2 have been shown in the previous section. A generalized form of the same is given in (4.4), to calculate the ϕ_i's for any set point in Phase-s.

$$\begin{aligned} &\phi_s = sin^{-1}(h - (s-1)lsin\theta_{to}/l) \\ &\phi_{s-1} = \theta_{to} - \phi_s \\ &\phi_i = 0 \quad \forall i \in n \backslash \{s, s-1\} \end{aligned} \tag{4.4}$$

The joint trajectories thus obtained are used to evaluate the static stability equations of the n-module robot as shown below:

$$
\begin{aligned}
&\sum F_x = 0 && N_1 - \sum_{i=s+1}^{n} F_i = 0 \\
&\sum F_y = 0 && 2(n+1)w_w + nw_l - 2F_1 - \sum_{i=s+1}^{n} N_i = 0 \\
&\sum M_{J_1} = 0 && 2F_1 r + (2F_1 - 2w_w) l cos\theta_1 \\
& && - w_l[(l/2)cos\theta_1 - csin\theta_1] \\
& && + 2N_1 l sin\theta_1 - \tau_1 = 0 \\
&\sum M_{J_j} = 0 && \tau_{j-1} - \tau_j - w_l[(l/2)cos\theta_j - csin\theta_j] + \\
&\forall j \in \{2, s\} && [(j-1)(w_l + 2w_w) - 2F_1)(l + l0)cos\theta_j \\
& && + 2N_1 l sin\theta_j = 0 \\
&\sum M_{J_q} = 0 && 2F_q r + 2N_{q-1} l - 2w_w l - w_l(l/2) - \\
&\forall q \in \{n \backslash s\} && [(s+q-1)(2w_w + w_l)](l + l0) \\
& && - (2F_1 + 2\sum_{t=1}^{q-1} N_t)(l + l_0) + \tau_{q-1} - \tau_q = 0 \\
&\sum M_{W_{n+1}} = 0 && 2F_{n+1} r + 2F_n r + 2N_{n-1} l \\
& && - [2(2w_w + w_l) - 2F_1 - 2\sum_{t=s+1}^{n} N_t](l + l_0) \\
& && - 2w_w l - w_l(l/2) + \tau_{n-1} = 0
\end{aligned}
\tag{4.5}
$$

4.4.2 Estimation of h_{max} and $\mathbf{k}$

Section III describes in sufficient detail how the quasi-static analysis is performed for a 3-module robot. The same can be extended for an n-module robot. The number of quasi-static equations' sets are equal to the number of climbing phases s wherein the static-stability equations are satisfied for a given n-module robot. It can be noted that $s \in \{1, n\}$. The generalized quasi-static equations for an n-modular robot in Phase-s are given in (4.5), below:

The equations are evaluated at each intermediate height. The optimization procedure is carried out for all the set points until the quasi-static constraints are violated. This determines the maximum height, h_{max}, that the robot can climb without tipping over. Thereafter, the desired moments($\boldsymbol{\tau}$) that are obtained from the optimization procedure are least squares approximated to determine the stiffness values($\mathbf{k}$) for their respective joints.

4.4.3 Illustration of Methodology

In order illustrate the utility of the proposed approach, a compliant 5-module robot, with module-length 18cm, was designed and its climbing ability was tested on surface whose μ value is 0.8. Its climbing maneuver was divided into 5 phases(as $n = 5$) and the optimization procedure was carried out for set points of increasing heights. It was noticed that the constraints were violated at a height of 50cm, i.e., in Phase-3 of its climbing maneuver. Subsequently, the methodology was followed further, to determine the stiffness values at joints J_1 and J_2 as $k_1 = 0.24$, $k_2 = 0.29$ and $k_3 = 0$, respectively. Figure 4.9 shows the snapshots of the 5-module robot successfully climbing a height of 36cm, viz., nearly two times the modules length. However, as observed in the case of the 3-module robot, the 5-module robot was also unable to lift its remaining modules for heights greater than 36cm.

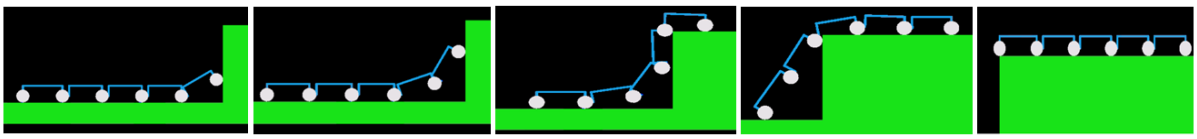

Figure 4.9 A 5 module compliant robot with compliant joints at J_1 and J_2 climbs a height of 36cm

The quasi-static analysis was carried out for compliant robots having upto 5-modules. It was observed that, for a height proportional to s link lengths, one additional module was sufficient to push the robot to reach the height. However, for the robot to successfully climb over the step, two additional modules were required. Though this illustration may hold true only for the multi-module robot discussed in this work, the methodology can be used to analyze any multi-module robot design.

4.5 Conclusions

In this chapter, compliant joints are fitted to a passive modular robot to enable it to climb step heights upto three times its wheel diameter. The detailed joint design procedure is shown and it is extended to designing compliant joints for an n-module robot to climb any given step height. The analysis of this robot design shows that compliant joints are very effective at re-distributing normal force to climbing wheel-pairs, resulting in a more efficient climbing behavior. Extensive numerical simulations are carried out to validate climbing performance both on steps and on general unstructured terrain.

While the addition of the springs ensures that the robot successfully climbs big obstacles, it does not guarantee that wheel-slip is minimum. Hence, a proper control of wheel torques can

help in slip minimization and power reduction. In the next chapter, the causes of wheel-slip are discussed and an optimization problem is formulated to avoid slippage.

Chapter 5

Augmented Traction Controller based on Wheel Torque Optimization

The compliant modular robot exhibited very good obstacle climbing ability and a generic method to extend it to climb any height was shown in the previous chapter. The design is extremely compact, lightweight and robust to minor changes in the environment. However, since it is wheeled robot containing a wheel-pair per module, wheel-slip can cause considerable energy loss and odometric errors. Before developing a controller to mitigate wheel-slip, the causes for slip are first studied.

Figure 5.1 shows the free-body diagram of a wheel rolling on a flat surface. The wheel is in static equilibrium when $F = \tau/r$, where r and τ are the wheel's radius and torque, respectively. For the wheel to maintain pure rolling, the frictional force $F = \mu_s N$, where μ_s is the coefficient of static friction. As F is proportional to τ, the wheel begins to slip if $F > \mu_s N$. Hence, the aim is always to keep the wheel torque less than $\mu_s N$. However, this is difficult to achieve as μ is not known beforehand, and it changes during robot's traversal. In automobiles, a well-known slip reduction technology, named, Anti-Lock Braking System (ABS), is used for minimizing

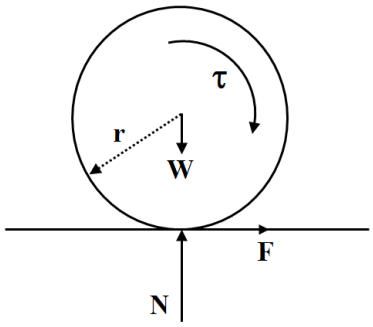

Figure 5.1 Free body diagram of the wheel

slip. It uses sensors to detect wheel-slip and then takes a corrective torque control measure to stop slip. Hence, this method requires slip to occur. On the other hand a preventive method, which is not only robust but also exploits the robot's suspension mechanism is desirable for slip minimization. Optimizing wheel torques with an objective to minimize slip could be a potential solution to this problem.

5.1 Wheel Torque Optimization

Wheel torque optimization is a very active research area, and its successful applications have been reported in [20, 18]. However, in their robots, all the wheels maintain contact with the ground throughout the traversal. On the other hand, in the proposed compliant modular robot, this is not always true. This necessitates an optimization formulation that can be solved in a phased manner.

5.1.1 Optimization Objective

It is observed that a majority of slip occurs when the robot is climbing the rise of a step or any such steep obstacle. Therefore, slip reduction during this phase of its traversal, will considerably improve the robot's performance. To build this analysis, one may first begin by assuming that there is no slip, and then estimate the F_i and N_i values across various points on the terrain by minimizing $\sum_i F_i/N_i$ to achieve the objective of no slip. Denote the maximum value of the F_i/N_i ratio obtained from this optimization as μ_o. The mechanism with lower μ_o can traverse on a wider range of surfaces (whose μ_s w.r.t the wheel is between μ_o and 1) without slipping. This is the most intuitive objective function for the optimization procedure, as shown in (6.1). However, since the function is non-linear, it may get stuck in local optima. Note that, this objective function doesn't enforce all the wheel-pairs to maintain the same μ_o value. This can be enforced by using (6.2) instead. Though these two objective functions best capture the objective of this optimization procedure, they both are non-linear and may get stuck in local optima. The objective can be linearized by just minimizing the sum of traction forces, as shown in (6.3), instead of minimizing the sun of traction-to-normal ratios. Since this function is linear it is guaranteed to converge to a global optimum value. The relative merits of these three objective functions is further analyzed in the subsequent sections.

Hence, optimization is carried out for all the wheel-pairs at set points between 0 and h_{max}, where $h_{max} = 2lsin\theta_{to}$. The wheel torque optimization for both phases of climbing is formu-

lated as

$$\sum_{i=1}^{4} F_i/N_i \tag{5.1}$$

$$\sum_{i=1}^{4}(F_i/N_i - \mu_{avg})^2 \quad where,\ \mu_{avg} = \sum_{i=1}^{4} F_i/N_i/4 \tag{5.2}$$

$$\sum_{i=1}^{4} F_i \tag{5.3}$$

In the next subsection, a method is introduced to determine the robot's posture at any given height. Though this may be trivial in the case of a three module robot, it is very essential as the number of modules increase.

5.1.2 Posture Estimation

It is important to estimate posture of the robot at various heights during the climbing phase. The use of 2-links for climbing at any instant, allows the robot to climb steps/walls as high as $2lsin(\theta_{to})$(i.e., h_{max}) without tipping over. To estimate the postures, the step height is divided into n set points between 0 and h_{max}, each point separated by a distance of $0.01m$. The posture of the robot at all the set points is determined so that they can to used to derive the static equilibrium equations for that posture. For step heights that involve only one climbing link i.e., heights between 0 and $lsin(\theta_{to})$ (phase-1), the posture of the robot, in terms of the joint angles, can be determined as $\phi_1^j = sin^{-1}(h^j/l)$ and $\phi_2 = 0$. When $\phi_1 = 70^0$ ($phi_1 \approx \theta_{to}$) , i.e., after having climbed a height of 0.14m, the robot transits to phase-2. Wheel-pair-2 is lifted off the ground and the robot now has two climbing members. This process reduces ϕ_1 and increases ϕ_2 while ensuring that $\theta_1 \leq \theta_{to}$. The desired postures for the second phase can be obtained by running a simple optimization procedure for all the heights between $lsin_{to}$ and $2lsin_{to}$ as shown in (6.4). The objective function ensures the net change in the relative angles is minimized while moving from one set-point to the other. This is very important from the quasi-static point of view as a drastic change in posture with a small increase in height cannot be attained without taking the dynamics of the system into consideration.

$$\begin{aligned} \underset{\phi_1,\phi_2}{\text{minimize}} \quad & \sum_{i=1}^{2}(\phi_i^j - \phi_i^{j-1})^2 \\ \text{subject to} \quad & lsin(\phi_1 + \phi_2) + lsin(\phi_2) = h^j \\ & \phi_1 + \phi_2 \leq \theta_{to} \\ & 0 \leq \phi_1, \phi_2 \leq \theta_{to} \end{aligned} \tag{5.4}$$

This provides the posture desired from the robot at various set-points. The objective functions have to be minimized across all these set-points to study the robot's performance and localize potential regions for slippage.

5.1.3 Optimization Routine

The design variables are F_i's and N_i's of all the four wheels. For maintaining an arbitrary posture of the robot, the static equilibrium equations have to be satisfied at that posture. Thus, they form the equality constraints to this problem. These equations change from one phase to the other at the set point $lsin\theta_{to}$, to reflect the fact that the second wheel is lifted off the ground. These equations are already provided in Chapter 2. As the posture is predetermined for a given height, the equality constraints are linear. However, since some of the objective functions are non-linear, standard functions like $fmincon$ (of MATLAB) rely on a strong initial guess provided by the user to search for the globally optimal value. Providing a good initial guess is hard in this scenario as the optimization routine has to be run on all the set points and each one may have a good initial guess of its own. An alternative approach is to further compress the feasible region by tightly bounding the design variables using the knowledge of their properties and the desired objective. To this end, additional linear inequality constraints are added to the system to reduce the feasible region and ensure that the proximity of the obtained solution is as close to the global minimum as possible. Equation (6.5) is to restrict the optimal F/N ratio to always remain between 0 and 1 for all the wheels and at all the set points. Equation (6.6) bounds the wheel motor torques for all the wheels with their maximum values. Finally, the ratio will also decrease if normal N increases. Therefore, equations in (6.7) ensures that the search space consists of only regions where N increases or maintains atleast N_{avg}, viz. the normal force on a flat terrain. Additionally, for phase 2, F_2 and N_2 are equated to 0 as wheel 2 is lifted off the ground and its traction no longer contributes to step climbing.

$$F_i \leq N_i \quad \forall\, i = 1 \ldots 4 \tag{5.5}$$

$$0 \leq F_i \leq \tau_{wmax}/r \quad \forall\, i = 1 \ldots 4 \tag{5.6}$$

$$\begin{aligned} phase\ 1: &\quad N_i \geq N_{avg} \qquad i \in \{2, 3, 4\} \\ phase\ 2: &\quad N_i \geq N_{avg} \qquad i \in \{3, 4\} \end{aligned} \tag{5.7}$$

The above mentioned optimization routine is performed for step of height 0.310m and at all its intermediate set points. The results are presented and discussed in the next section.

5.2 Optimization Results and Discussion

Wheel torque optimization is carried out using the three objective functions as given in (6.1),(6.2) and (6.3) at all the set points between 0 and h_{max}. The traction-to-normal force ratios for all the wheel pairs are plotted against the height set points, as shown in Fig.5.2. It can be seen clearly that none of the objective functions yield F/N values that are consistent across heights and across wheel-pairs. It is interesting to note that Objective-2 maintained some consistency through a climbing phase. However, there is a sharp change in the values when it transits from one climbing phase to another.

During the initial stages of climbing, $F_3/N_3 \approx 1$ in all the three cases. This implies that wheel-pair 3 have every chance of slipping as the robot begins to climb. Though this large value is touched upon during some set points in the beginning, all other wheel ratios are considerably lower across objective functions. This makes μ_o alone an inefficient metric to assess the performance of the robot. Keeping this in view, two additional metrics are used, namely Mean and Mode of the traction-to-normal force ratios for all the wheel-pairs, across height set-points, per objective function. The values thus obtained are listed in the Table 5.1. It is very counter-intuitive to note that objective-2 (given by (4)) performs poorly on all the metrics. This could be due to the highly non-linear nature of the function, making it most susceptible to settling at local minima. It is equally interesting to note that objective function-3 (given in (5)) is also not the best objective function in spite of being linear and having global optima guarantees. Objective-1 (given by (3)) performs consistently well on all the metrics. It may be noted that Objectives-1 and -3 perform very similarly in climbing phase-1. However in phase-2, objective-1 performs significantly better, as seen in Figs. 5.2-(a) and 5.2-(c). This can also be verified from the optimal wheel torque plots shown in Fig. 5.6. It can be clearly seen that wheel torques in Fig.5.6-(c) may saturate sooner that those in Fig. 5.6-(a). Thus, Objective-1 is finalized as the desired objective function. We now examine the optimal traction-to-normal force ratios and optimal wheel torques obtained using objective-1 to better understand its behavior.

Objective Function	Max. value (μ_o)	Mean	Mode
Objective-1	1.0017	0.1464	0.0023
Objective-2	1.0593	0.3887	0.0030
Objective-3	1.0018	0.1926	0.0029

Table 5.1 Objective Functions Analysis

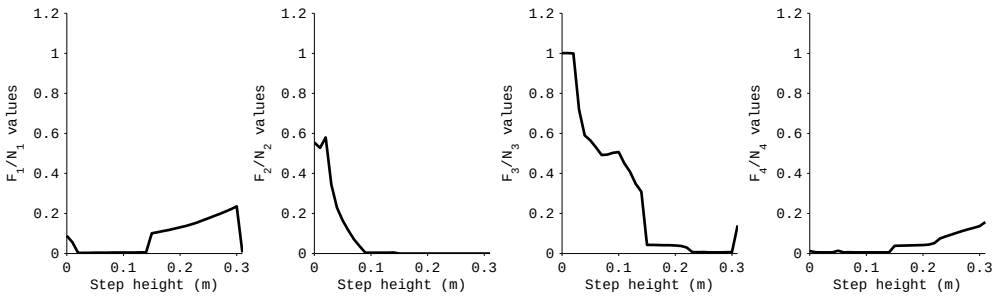

(a) Objective-1

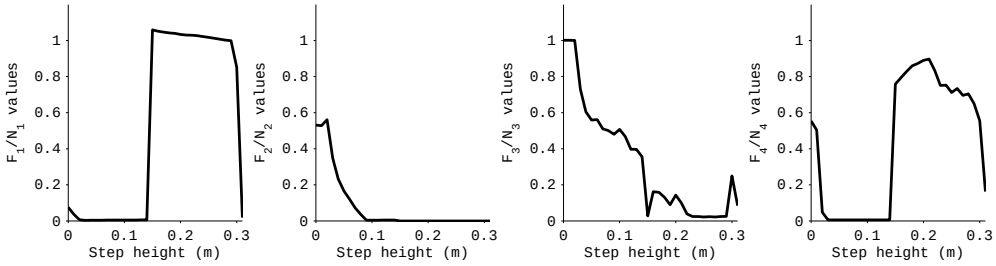

(b) Objective-2

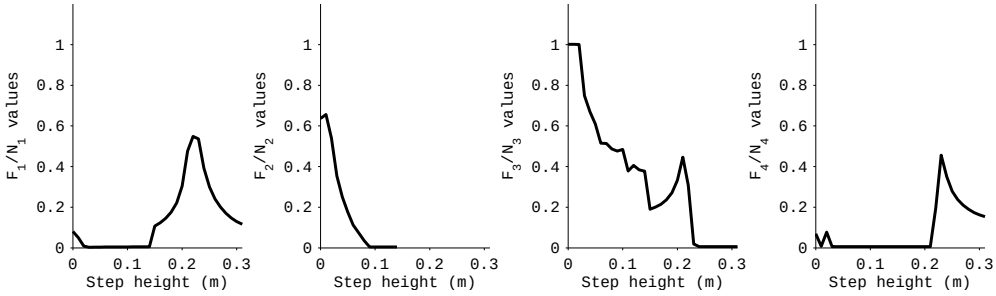

(c) Objective-3

Figure 5.2 Optimized F/N values for all the four wheel-pairs using the three objective functions

It can be noted from Figure 5.2(a) that, for wheel-pair-1, the F/N ratio is consistently lower (max F_1/N_1 = 0.2357) as compared to all other wheels and especially lower in phase-1. In phase-1, all the three wheel torques combine to provide the horizontal normal force N_1. Thus, N_1 is always greater than or equal to $3N_{avg}$. Even though the required wheel torque for rolling might remain the same while climbing the step, the normal force has more than tripled thus greatly reducing F_1/N_1. This implies that this robot can climb on a very slippery surface without slipping as the reduction in μ_s is being compensated by increase in normal force N. This is the key novelty of modularity that this robot design wishes to exploit. For phase-2 however, the normal force $N_1 \geq 2N_{avg}$. Therefore, this robot can climb a step without slipping

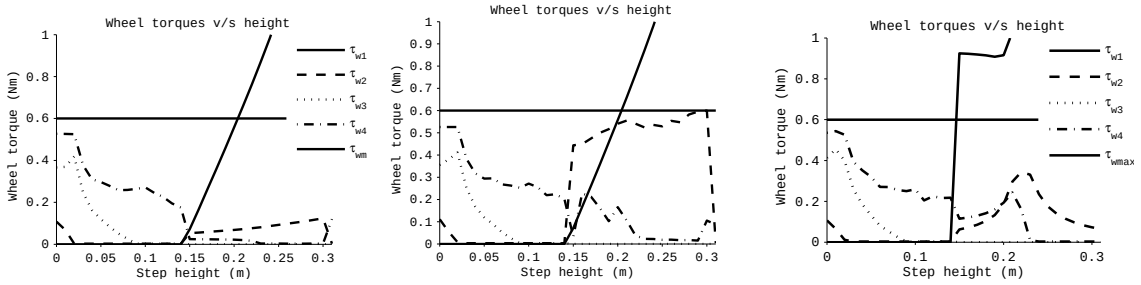

(a) (b) (c)

Figure 5.3 Optimal wheel torque plots for all the wheel pairs with a) objective function-1, b) objective function-2 and c) objective function-3

even if μ_s drops to a third of its original value in phase-1 or to half its value in phase-2. This makes this robot mechanism robust to changes in μ_s during step climbing. For wheel-pair-2, however, F_2/N_2 reduces with an increase in height. However, in phase-2, wheel-pair-2 is not actuated as it can no longer provide traction. For wheel-pair-3, as shown in Figure 5.2(c), a trend similar to that of wheel-pair-2 is observed. It starts decreasing appreciably in phase-2 when wheel-pair-2 is off the ground as N_3 increases. Wheel-pair-4 has a counter intuitive trend. The average F_4/N_4 value is 0.0483 which is very low. However, the ratio increases in phase-2 instead of decreasing as in the case of other wheels. When the second wheel-pair is lifted off the ground, to maintain static equilibrium in the x-direction, forces are redistributed thus increasing the values of F_3 and F_4. However, for wheel-pair-3, N_3 also increases accordingly and therefore the ratio could be kept lower. The normal force N_4, on the other hand, doesn't increase proportionally thus increasing the ratio in the case of wheel-pair-4.

Note that the optimal wheel torque obtained so far only maintain the robot in static equilibrium at a given height. However, the robot has to be imparted with some motion to move from one set-point to another. Additional torque needs to be applied to move the robot with a desired velocity. Therefore, a velocity controller is coupled to these optimal wheel to obtain the desired optimal wheel torque controller as described in the next section.

5.3 Proposed Wheel Torque Controller Design

Optimal wheel torque control is a very active research area and several instances of successful application of wheel torque control for mobile robots, like SHRIMP [10] and CRAB [26], have been reported earlier in [22], [21], [19], [18]. A detailed study of this method is given in [20]. Generally, robots that traverse on uneven terrains move with speeds in the range of $5 - 20cm/s$ [22]. At such low speeds the dynamic effects are minimal, and hence, a controller

can be developed based on the optimal wheel torques, already obtained with the quasi-static assumption. Moreover, to move the robot forward, some velocity has to be provided. For this, a velocity control is also combined with the optimal wheel-torques. The fusion of the two will be referred to as torque control, hereafter. This will enable the wheel to generate traction force(F) within its upper bound (μN), and minimizes the risk of slippage. Note that at every iteration the state of the robot is used to determine the optimal wheel torques among all the wheels. These values are then combined with the torque values obtained from the velocity feedback loop to generate the necessary wheel torques for robot's motion. The block diagram of the proposed controller is shown in Fig. 5.4, where s denotes the state of the robot, V_m and V_d denote the measured and desired wheel velocities, e denotes the velocity error term, and τ_o, τ_v and τ_c denote the torque values obtained from the optimizer, velocity controller, and normal force based distribution, respectively.

It is worth noting that the normal forces (N) are used to augment the application of τ_v to all the wheels, as shown in Fig. 5.4. Due to this, the wheels can apply higher torques when the normal forces are higher. This helps in taking the burden off the wheels with lower normal forces, and further reducing slippage. This also ensures that $\tau_{v_i} = 0$ when the i^{th} wheel loses contact with the ground, thus saving power. In Fig. 5.4, τ_c denotes the corrected torque for each individual wheel for achieving the desired velocity. Note that, while this process may hinder a wheel from achieving the desired velocity, it still achieves the larger goal of generating forward motion with minimal slip.

The utility of the proposed torque control is compared to the conventional velocity control, and the net reduction in slip ratio and torque requirement is estimated. Numerical experiments were conducted in a multibody dynamics software (MSC ADAMS). Later, it was implemented on the prototype of the compliant modular robot.

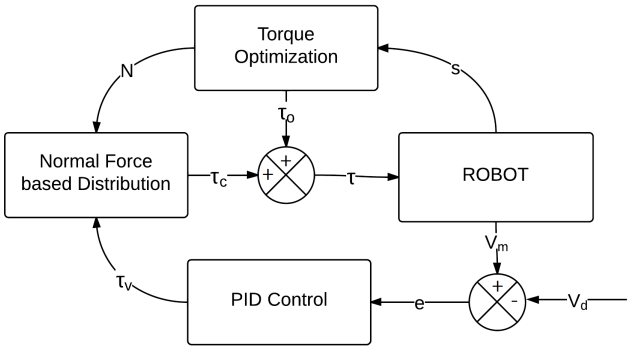

Figure 5.4 Block diagram of the proposed controller

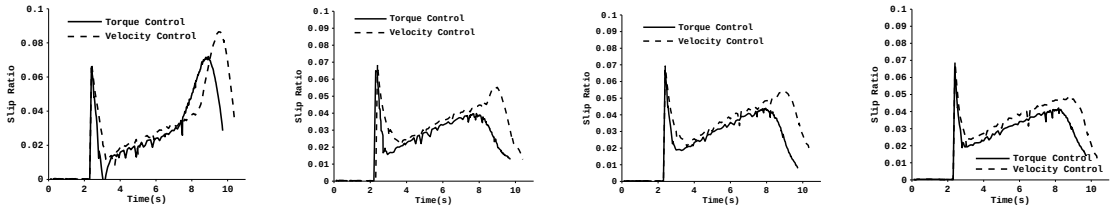

Figure 5.5 Slip ratios of wheel-pairs 1-4 on a surface with $\mu = 0.8$ using both velocity control and torque control.

Two metrics were used to study the performance of the robot. They are average slip ratio(s_a) and mean wheel torque ($\overline{T}$). Slip ratio is given by, $1 - v/r\omega$, where v is the linear velocity of each wheel and ω is the angular velocity measured by wheel encoder. The slip ratios of all the wheels were determined and averaged to obtain the Average Slip Ratio. Similarly, the wheel torques for all the wheels were measured and averaged to obtain the Mean Wheel Torque $\overline{T}$. The robot was tested on a wide range of terrains, and its performance was studied in the following subsections.

5.3.1 Numerical Results

In the numerical simulations, the robot was made to climb a step of height $14cm$, which is more than twice the wheel diameter. Note that the maximum wheel slip occurs in the robot while climbing the rise of a step. Therefore, the average slip ratio and mean torque requirement were measured for all the wheels during the step climbing phase. The coefficient of friction μ of the wheel-ground contact was varied between $0.6 - 1.0$ and several test runs were taken to study the climbing behavior of the robot. The slip ratio results for all the wheel-pairs when $\mu = 0.8$ are shown in Fig. 5.5. A reduction of 34%,16%,16% and 23% was observed in the slip ratios of wheel-pairs 1-4. Similar trend was observed at other values of μ. It was shown earlier in [4] that wheel-pairs 1 and 4 would be least susceptible to slip when optimal torque values are applied. The simulations are clearly in agreement with the analysis made using the results of the optimization procedure.

It is worth noting that the robot climbs the step faster when it uses torque control. There are two reasons for this, firstly, the optimal torques obtained from the optimization procedure ensure that the system is statically balanced. This implies that the velocity control needs to apply only the necessary torque to achieve the desired velocity. Secondly, τ_c enables the wheels with higher normal forces to apply greater traction. It was shown in [5] that, due to the spring

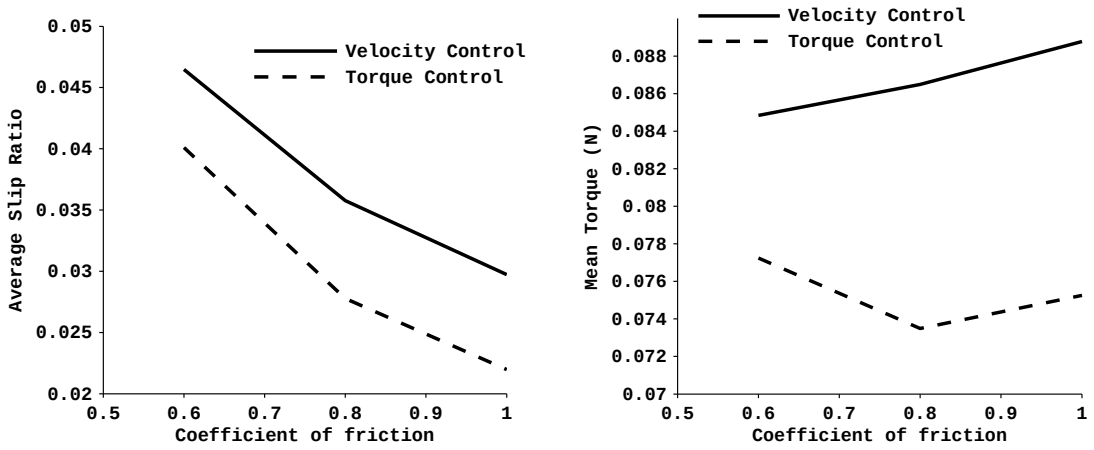

Figure 5.6 Plots for average slip ratio and mean torque, with μ varying between $0.6 - 1.0$, using both velocity control and torque control.

compliance, the normal force N_1 increases as wheel-pair 1 climbs the rise of the step. Consequently, wheel-pairs will require less time to climb the step, especially wheel-pair 1.

The results of average slip ratio and mean wheel torque for different values of coefficient of friction are shown in Table 5.2 and in Fig. 5.6. It can be seen that there is a considerable reduction in overall wheel-slip when torque control is implemented. There is also a decrease in the average torque requirement. Motivated by the above results, torque control was also implemented on the prototype of compliant modular robot, and its effectiveness is shown in the following subsection.

Table 5.2 Results for Average Slip Ratio and Mean Torque

	Average Slip Ratio			Mean Wheel Torque (Nm)		
μ value	Velocity Control	Torque Control	% change	Velocity Control	Torque Control	% change
0.6	0.046	0.040	13.71	0.084	0.077	8.95
0.8	0.035	0.027	22.37	0.086	0.073	15.03
1	0.029	0.021	26.04	0.088	0.075	15.23

5.4 Conclusions

This chapter presents an optimal wheel torque based controller for a compliant modular robot. An optimization problem is formulated that aims to minimize wheel-slip, leading to better control and energy efficient climbing. It has been shown through numerical studies that the controller leads to considerably lower slip ratios and torque requirement while climbing step-like obstacles when compared to the conventional velocity control. Though this approach can be easily extended to locomotion on uneven terrain, since the robot is not equipped with any sensory mechanism for contact angle detection, the analysis in this chapter is limited to step climbing. However, it may be noted that a significant amount of wheel-slip occurs while climbing steep obstacles. Therefore, a comprehensive analysis of the torque control method is shown here by testing its utility on various surfaces and verifying its versatility.

Chapter 6

Prototype Development and Testing

6.1 Introduction

A prototype of the 3-module compliant robot is developed, as shown in Figs.6.1(a)-(b). The brief overview of the mechanical and electrical designs are provide below:

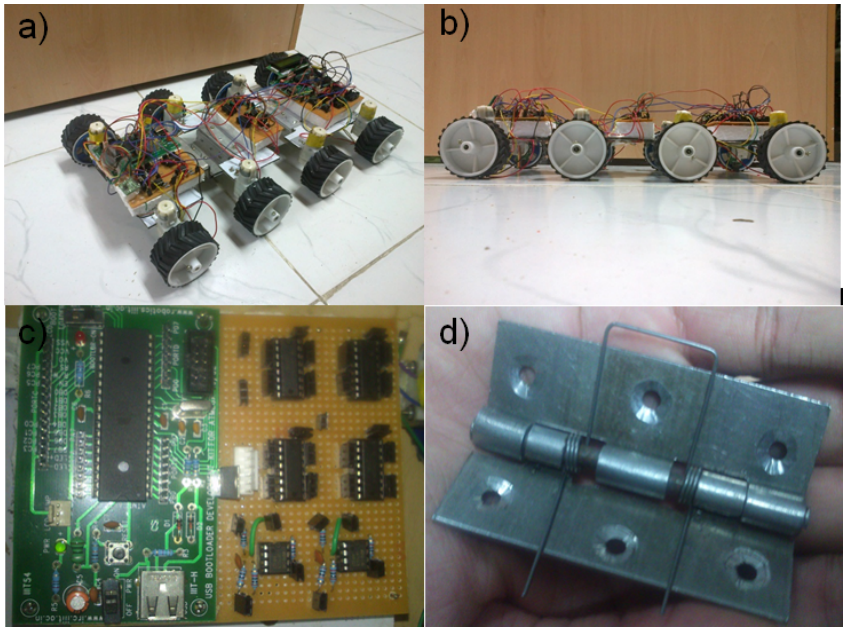

Figure 6.1 Details of the Prototype: (a) and (b) show the isometric and front views of a 3 module robot; (c) the novel compliant joint and (d) customized controller board developed for the prototype

6.1.1 Mechanical Design

Each module of the robot consists of an Aluminum base, dimensions of which are given in Table I. Two high grip wheels are fitted on both sides of the module. The torsional spring at the joint J_1 designed as per the stiffness values obtained in the previous section, and fitted directly into the hinge as shown in Fig. 6.1(d). The spring is a double helical with 3 coils on either side and made of 1mm diameter fine grained steel wire. The inner diameter of each coil is 2 cm while the arm length is 2.5 cm from the axis of the spring. The free angle is fixed at 90^0. Spring is connected only to the second module, and it maintains a free contact with the first module. It resists counter clockwise moment at the joint J_1, and helps in avoiding tip over. The free contact on one side, helps in freely deforming along the obstacle without exerting any moment.

6.1.2 Electrical Design

Each wheel-pair is driven by two geared DC motors (Solarbotics GM3 variant). The motors contain 224:1 gearheads and offer a stall torque of 4 kg-cm at 9V. In addition to the motors, the wheels are fitted with Nubotics Wheel Watchers (WW-12) quadrature encoders with a resolution of 128 clocks per rotation. The robot also contains a customized AtMega 16 development board (shown in Fig. 6.1(c)) which is used for implementing the various control methodologies that are going to be realized on the robot. Each motor has an L293D motor driver. The robot is also equipped with Sharp GP2Y0A21YK IR sensor on the first module, offering a reasonable 24 cm range, for obstacle detection. A 3-axis accelerometer (ADXL335) is also used for tilt and slip rate estimations.

6.2 Compliant Robot Prototype in Action

Extensive simulations were carried out to demonstrate the effectiveness of compliant joints in avoiding tip over and improving the robot's step climbing ability. The results are already reported in Section-III. Figures 4.3, 4.4 and 4.5 show that, the use of springs has not only helped in avoiding tip-over but it also increased the normal force at the climbing wheel-pair's contact and enabled it to generate more traction without slipping. In order to validate the simulation results, an experimental prototype of a compliant robot was developed. Its climbing ability was assessed on different types of obstacles, first numerically, and then experimentally. Their details are presented in the following subsections.

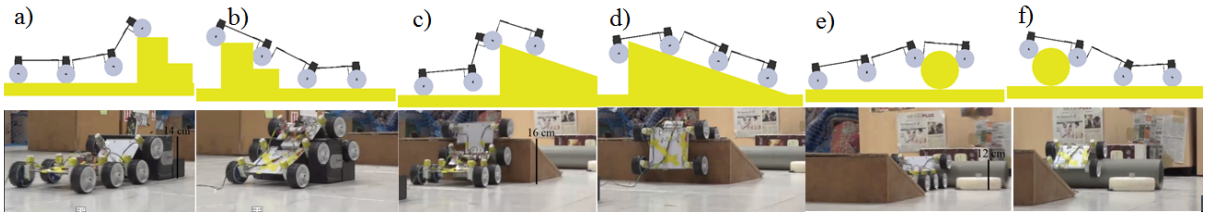

Figure 6.2 Demonstrating the climbing ability of the 3-module robot in simulation (top row) and experiment (bottom row): In a)-b), the obstacle is a rectangular block of 14 cm height; In c)-d), it is wooden ramp of maximum height 16 cm; Finally, in c)-d), the obstacle is a cylindrical pipe of 12 cm diameter

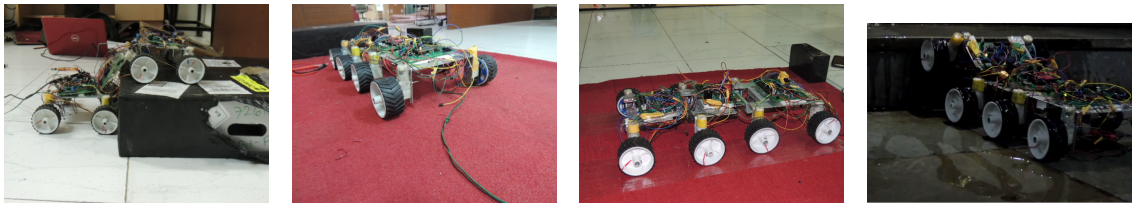

(a) (b) (c) (d)

Figure 6.3 Experiments on the prototype: The robot was made to climb on, a) Tiled , b) Carpeted ,c) Taped and d) Wet floors

The climbing ability of the robot with compliant joints was tested on an uneven terrain created using obstacles made of different materials and of varying heights. It was observed that the climbing ability of the robot improved remarkably with the addition of springs. The terrain consisted of a rectangular block of 14 cm height, a ramp of maximum height 16 cm and a cylindrical pipe of 12 cm diameter. The robot was able to successfully climb over all these obstacles. This validates the effectiveness of the proposed design of compliant robot.

6.3 Robot with Optimal Torque Controller

The robot is equipped with current sensors to measure the current drawn by the motors. As the motor torque is directly proportional to current $\tau = ki$, where k is motor constant, the mean torque required for climbing was measured through current readings. The wheel encoder readings were logged for all the test runs, and average linear velocity was measured by dividing distance traveled with the time taken. Inertial Measurement Units(IMUs) were used to estimate the states of links. All the sensors were integrated to an AtMega-16 development board, which was fabricated in-house.

The performance of the experimental prototype was tested on various types of wheel-ground interfaces. It was made to climb a step of height 14 cm. The robot was run on four types of slippery surfaces namely, tiled, carpeted, taped and wet, as shown in Fig.6.3(a)-(d). Sample torque readings for wheel-pairs 1 and 4 while traversing on the carpeted surface are shown in Fig. 6.4. The average slip ratio and mean torque values obtained for all surfaces are tabulated in Table 6.1. There is a significant reduction in the wheel-slip, which validates the simulation results. This shows the efficacy of the proposed approach.

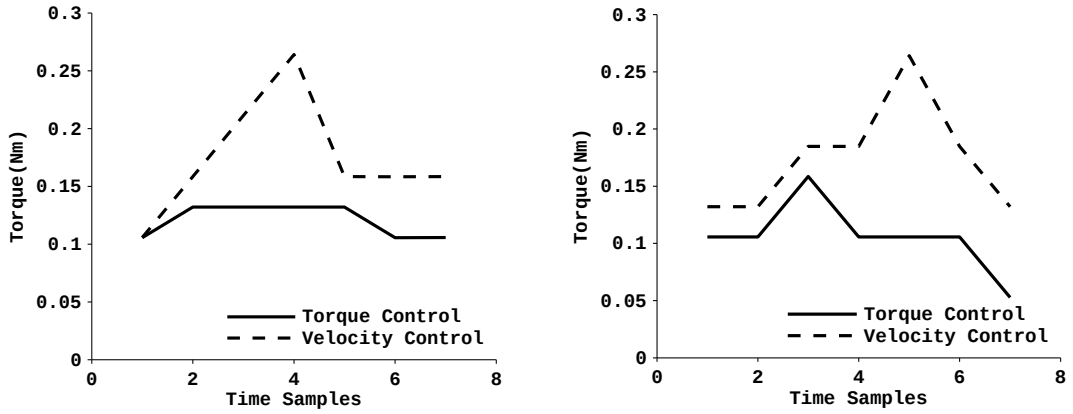

Figure 6.4 The torque values at wheel-pairs 1 and 4 while climbing the rise of the step on a tiled floor

Table 6.1 Experimental results for average slip ratio and mean torque

	Average Slip Ratio		Mean Torque (Nm)	
Floor Type	Velocity Control	Torque Control	Velocity Control	Torque Control
Tiled	0.188	0.0532	0.0867	0.0624
Carpeted	0.204	0.082	0.0796	0.0662
Taped	0.28	0.237	0.0799	0.0674
Wet	0.238	0.169	0.0724	0.0697

6.4 Conclusions

In this chapter, the prototype construction details are provided. The theories developed in Chapters 4 and 5 are implemented on the prototype. The prototype successfully climbs an obstacle of height 18 cm. It also shows good climbing ability on a general unstructured terrain. The robot is made to climb steps having different surface properties like tiled, carpeted, taped and wet to verify the robustness of the torque controller to changes in the wheel-ground interactions. The use of optimal wheel torque control also shows significant reduction in wheel-slip, thus validating the numerical results obtained in the last chapter.

Chapter 7

Conclusions

In this work, we present a novel modular robot mechanism for climbing big step-like obstacles. Conventional robot mechanisms developed for rough terrain navigation have limited obstacle climbing ability which is generally limited to twice their wheel diameter or link height. However, in Urban Search and Rescue situations, it is generally very difficult to estimate in advance, the heights of obstacles. Therefore, a more versatile robot is essential to cover maximum ground. The first solution proposed a five module semi-active robot that showed augmented climbing ability. It climbed obstacles that were upto twice its link length. However, it couldn't be extended to bigger heights without adding additional actuators.

The second solution proposed the use of compliant joints. The use of actuators for configuration control is fully eliminated. An optimization problem based on the robot's static model is used to estimate joint stiffness. A three module prototype is shown to successfully climb a 17 cm obstacle, which is thrice its wheel diameter. This is one of the highest reported for passively articulated systems. Additionally, a generalized methodology is proposed to estimated the maximum height that can be climbed using a n module robot. Using this methodology, it was shown that a 5 module robot can climb a height of 36 cm, which is six times its wheel diameter. Compliant joints are shown to not only avoid tip-over but also improve the robot's climbing performance by redistributing the normal forces to enable climbing wheels to apply greater traction. This discussed in detail through extensive numerical results.

Additionally, an optimal wheel-torque based controller is developed for robot locomotion. The aim of this new controller is to minimize wheel-slip and improve energy efficiency and wheel odometry accuracy. The objective of this optimization is to minimize the traction-to-normal force ratios for all the wheels during the step climbing phase. The efficacy of the controller was tested extensively both numerically and experimentally. The robot was made to climb a step on different surfaces, like wet, carpeted, tiled, etc. The mean torque requirement and mean slip rate for all the wheels were computed for all the test cases. Significant reduction

in mean torque(as high as 26%) and mean slip rate (as high as 15%) were noted. This validates the utility of this controller.

7.1 Future Work

- The major focus of future work is to equip the robot with compliant yaw and roll joints to augment its mobility on a $3D$ unstructured terrain.
- During the numerical studies, it was noted that the optimal spring stiffness values are task specific(step ascent, descent, trench crossing, etc.) and joint specific(they vary for J_1 ,J_2, etc.). Therefore to dynamically vary spring stiffness during traversal, the use of parallel/series elastic actuators will be explored.
- Latching mechanisms need to be developed for actively attaching and detaching modules, when required, to achieve reconfigurability.

Bibliography

[1] Dimitrios Apostolopoulos. Analytic configuration of wheeled robotic locomotion. 2001.

[2] Masayuki Arai, Toshio Takayama, and Shigeo Hirose. Development of souryu-iii: connected crawler vehicle for inspection inside narrow and winding spaces. In *IEEE/RSJ International Conference on Intelligent Robots and Systems (IROS)*, 2004.

[3] Masayuki Arai, Yoshinori Tanaka, Shigeo Hirose, Hiroyuki Kuwahara, and Shingo Tsukui. Development of souryu-iv and souryu-v: serially connected crawler vehicles for in-rubble searching operations. *Journal of Field Robotics*, 2008.

[4] Siravuru Avinash, Suril V Shah, and K Madhava Krishna. Wheel torque optimization for a compliant modular robot. In *National Conference on Machines and Mechanisms (NaCoMM), Roorkee, India*, 2013.

[5] Siravuru Avinash, Ankur Srivastava, Akshaya Purohit, Suril V Shah, and K Madhava Krishna. A compliant multi-module robot for climbing big step-like obstacles. In *IEEE International Conference on Robotics and Automation (ICRA), Hong Kong, China*, 2014.

[6] Alexander S Boxerbaum, Julio Oro, Gilbert Peterson, and Roger D Quinn. The latest generation whegs robot features a passive-compliant body joint. In *IEEE/RSJ International Conference on Intelligent Robots and Systems (IROS)*, 2008.

[7] H. Benjamin Brown, J.M. Vande Weghe, C.A. Bererton, and P.K. Khosla. Millibot trains for enhanced mobility. *Mechatronics, IEEE/ASME Transactions on*, 2002.

[8] A. Davids. Urban search and rescue robots: from tragedy to technology. *IEEE Intelligent Systems*, 17(2):81–83, 2002.

[9] Ashish Deshpande and Jonathan Luntz. Behaviors for physical cooperation between robots for mobility improvement. *Autonomous Robots*, 2007.

[10] T. Estier, Y. Crausaz, B. Merminod, M. Lauria, R. Piguet, and R. Siegwart. An innovative space rover with extended climbing abilities. *Proceedings of Space and Robotics*, 2000:333–339, 2000.

[11] Erico Guizzo. Japan earthquake: More robots to the rescue. *IEEE Spectrum*, 2011.

[12] Erico Guizzo. Japan earthquake: Robots help search for survivors. *IEEE Spectrum*, 2011.

[13] Shigeo Hirose, Takaya Shirasu, and Edwardo F Fukushima. Proposal for cooperative robot gunryu composed of autonomous segments. *Robotics and Autonomous Systems*, 1996.

[14] Shigeo Hirose and Hiroya Yamada. Snake-like robots [tutorial]. *IEEE Robotics & Automation Magazine*, 2009.

[15] Tetsushi Kamegawa, Tatsuhiro Yamasaki, Hiroki Igarashi, and Fumitoshi Matsuno. Development of the snake-like rescue robot. In *IEEE International Conference on Robotics and Automation (ICRA)*, 2004.

[16] A. Kamimura and H. Kurokawa. High-step climbing by a crawler robot dir-2-realization of automatic climbing motion. In *IEEE/RSJ International Conference on Intelligent Robots and Systems (IROS)*, 2009.

[17] Hitoshi Kimura and Shigeo Hirose. Development of genbu: Active wheel passive joint articulated mobile robot. In *IEEE/RSJ International Conference on Intelligent Robots and Systems (IROS)*, 2002.

[18] Ambroise Krebs, Fabian Risch, Thomas Thueer, Jérôme Maye, Cédric Pradalier, and Roland Siegwart. Rover control based on an optimal torque distribution-application to 6 motorized wheels passive rover. In *IEEE/RSJ International Conference on Intelligent Robots and Systems (IROS), Taipei, Taiwan*, 2010.

[19] Ambroise Krebs, Thomas Thueer, Edgar Carrasco, and Roland Siegwart. Towards torque control of the crab rover. In *Proceedings of the 9 th International Symposium on Artificial Intelligence, Robotics and Automation in Space (iSAIRAS), Los Angeles, USA*, 2008.

[20] Ambroise Krebs, Thomas Thueer, Stéphane Michaud, and Roland Siegwart. Performance optimization of all-terrain robots: a 2d quasi-static tool. In *IEEE/RSJ International Conference on Intelligent Robots and Systems (IROS), Beijing, China*, 2006.

[21] P. Lamon and R. Siegwart. Wheel torque control in rough terrain-modeling and simulation. In *IEEE International Conference on Robotics and Automation (ICRA), Barcelona, Spain*, 2005.

[22] Pierre Lamon, Ambroise Krebs, Michel Lauria, Roland Siegwart, and Steven Shooter. Wheel torque control for a rough terrain rover. In *IEEE International Conference on Robotics and Automation (ICRA), New Orleans, USA*, 2004.

[23] Elena Messina and Adam Jacoff. Performance standards for urban search and rescue robots. In *Defense and Security Symposium*, 2006.

[24] Arun Kumar Singh, Rahul Kumar Namdev, Vijay Eathakota, and K Madhava Krishna. A novel compliant rover for rough terrain mobility. In *IEEE/RSJ International Conference on Intelligent Robots and Systems (IROS)*, 2010.

[25] Kousuke Suzuki, Atsushi Nakano, Gen Endo, and Shigeo Hirose. Development of multi-wheeled snake-like rescue robots with active elastic trunk. In *IEEE/RSJ International Conference on Intelligent Robots and Systems (IROS)*, 2012.

[26] Thomas Thueer, Pierre Lamon, Ambroise Krebs, and Roland Siegwart. Crab-exploration rover with advanced obstacle negotiation capabilities. In *Proceedings of the 9th ESA Workshop on Advanced Space Technologies for Robotics and Automation (ASTRA), Noordwijk, The Netherlands*, 2006.

[27] K. Turker, I. Sharf, and M. Trentini. Step negotiation with wheel traction: a strategy for a wheel-legged robot. In *IEEE International Conference on Robotics and Automation (ICRA), St. Paul, USA*, 2012.

[28] Bin Xu, Cedric Pradalier, Ambroise Krebs, Roland Siegwart, and Fuchun Sun. Composite control based on optimal torque control and adaptive kriging control for the crab rover. In *IEEE International Conference on Robotics and Automation (ICRA), Shanghai, China*, 2011.

[29] Hiroya Yamada and Shigeo Hirose. Development of practical 3-dimensional active cord mechanism acm-r4. *Journal of Robotics and Mechatronics*, 2006.

[30] Brian Yamauchi. Packbot: A versatile platform for military robotics. In *Proc. SPIE*, 2004.

[31] Mark Yim, David G Duff, and Kimon Roufas. Modular reconfigurable robots, an approach to urban search and rescue. In *1st International Workshop on Human-friendly Welfare Robotics Systems*, 2000.

[32] Mark Yim, Sam Homans, and Kimon Roufas. Climbing with snake-like robots. In *IFAC Workshop on Mobile Robot Technology*, 2001.

[33] Mark Yim, Wei-Min Shen, Behnam Salemi, Daniela Rus, Mark Moll, Hod Lipson, Eric Klavins, and Gregory S Chirikjian. Modular self-reconfigurable robot systems [grand challenges of robotics]. *IEEE Robotics & Automation Magazine*, 14(1):43–52, 2007.

[34] Mark Yim, Wei-Min Shen, Behnam Salemi, Daniela Rus, Mark Moll, Hod Lipson, Eric Klavins, and Gregory S Chirikjian. Modular self-reconfigurable robot systems [grand challenges of robotics]. *IEEE Robotics & Automation Magazine*, 2007.

Chapter 8

Appendix

1. Notations

l	$Length\ of\ the\ trunk$
l_0	$Offset\ distance\ between\ trunk-joint\ and\ wheel\ joint$
c	$Clearance\ between\ wheel\ center\ and\ trunk$
r	$Radius\ of\ the\ wheel$
ϕ_i	$Relative\ angle\ between\ links\ i\ and\ i+1$
m_l	$Mass\ of\ the\ trunk$
m_w	$Mass\ of\ the\ wheel$
L	$Weight\ of\ the\ trunk\ (m_l g)$
W	$Weight\ of\ the\ wheel\ (m_w g)$
fx_{li}	$X\ component\ of\ the\ trunk-joint\ reaction\ force\ between\ trunks\ i\ and\ i+1$
fy_{li}	$Y\ component\ of\ the\ trunk-joint\ reaction\ force\ between\ trunks\ i\ and\ i+1$
fx_{wi}	$X\ component\ of\ the\ wheel-joint\ reaction\ force\ on\ the\ trunk\ due\ to\ wheel\ i$
fy_{wi}	$Y\ component\ of\ the\ wheel-joint\ reaction\ force\ on\ the\ trunk\ due\ to\ wheel\ i$
τ_{wi}	$Torque\ applied\ at\ wheel\ i$
k_i	$spring\ constant\ of\ spring\ i$

2. Free Body diagrams for the One Link Climbing Case

   (a) Module 1

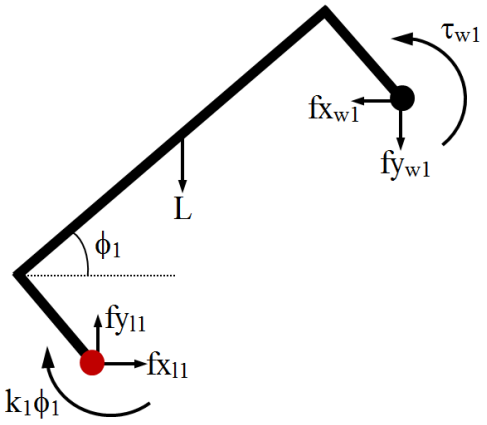

(a) Trunk 1

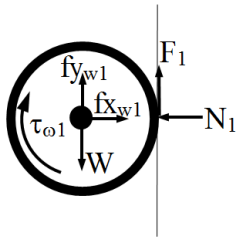

(b) Wheel 1

Figure 8.1

For Trunk 1,

$$fx_{l1} - fx_{w1} = 0$$

$$fy_{l1} - L - fy_{w1} = 0$$

$$k_1\phi_1 + L((l/2)cos\phi_1 - csin\phi_1) + fy_{w1}lcos\phi_1 - fx_{w1}lsin\phi_1 - 2\tau_{w1} = 0$$

For Wheel 1,

$$fx_{w1} - 2N_1 = 0$$

$$fy_{w1} - 2W + 2F_1 = 0$$

$$\tau_{w1} - F_1 r = 0$$

(b) Module 2

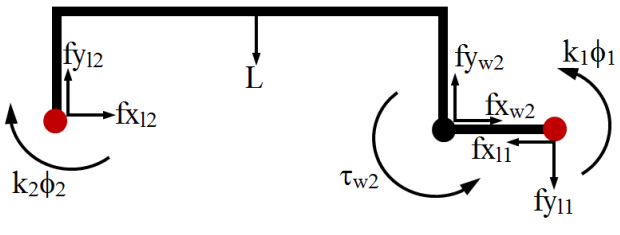

(a) Trunk 2

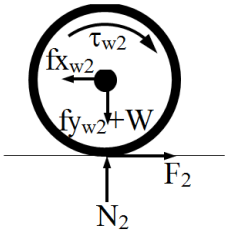

(b) Wheel 2

Figure 8.2

$$For\ Trunk\ 2,$$
$$fx_{l2} - fx_{l1} + fx_{w2} = 0$$
$$fy_{l2} + fy_{w2} - fy_{l1} - L = 0$$
$$k_2\phi_2 - k_1\phi_1 + L(l/2) +$$
$$fy_{l1}(l + l_0) - fx_{w2}l - 2\tau_{w2} = 0$$

$$For\ Wheel\ 2,$$
$$fx_{w2} - 2F_2 = 0$$
$$fy_{w2} - 2N_2 + 2W = 0$$
$$\tau_{w2} - F_2 r = 0$$

(c) Module 3

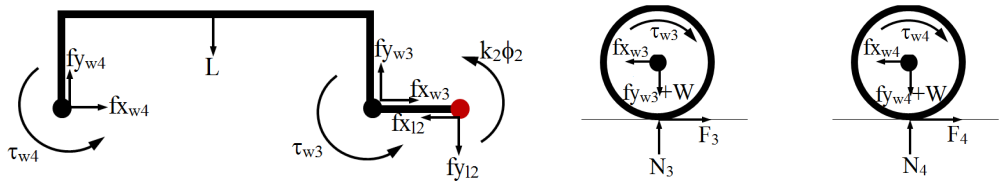

(a) Trunk 3 (b) Wheel 3 (c) Wheel 4

Figure 8.3

$$For\ Trunk\ 3,$$
$$fx_{l2} - fx_{w3} - fx_{w4} = 0$$
$$fy_{w4} + fy_{w3} - fy_{l2} - L = 0$$
$$L(l/2) + fy_{l2}(l + l_0) - k_2\phi_2$$
$$- fx_{w3}l - 2\tau_{w3} - 2\tau w4 = 0$$

$$For\ Wheel\ 3,$$
$$fx_{w3} - 2F_3 = 0$$
$$fy_{w3} - 2N_3 + 2W = 0$$
$$\tau_{w3} - F_3 r = 0$$

$$For\ Wheel\ 4,$$
$$fx_{w4} - 2F_4 = 0$$
$$fy_{w4} - 2N_4 + 2W = 0$$
$$\tau_{w4} - F_4 r = 0$$

3. Free Body diagrams for the Two Link Climbing Case

(a) Module 1

$$For\ Trunk\ 1,$$
$$fx_{l1} - fx_{w1} = 0$$
$$fy_{l1} - L - fy_{w1} = 0$$
$$k_1\phi_1 + L[(l/2)cos(\phi_1 + \phi_2) - csin(\phi_1 + \phi_2)] +$$
$$fy_{w1}lcos(\phi_1 + \phi_2) - fx_{w1}lsin(\phi_1 + \phi_2) - 2\tau_{w1} = 0$$

$$For\ Wheel\ 1,$$
$$fx_{w1} - 2N_1 = 0$$
$$fy_{w1} - 2W + 2F_1 = 0$$
$$\tau_{w1} - F_1 r = 0$$

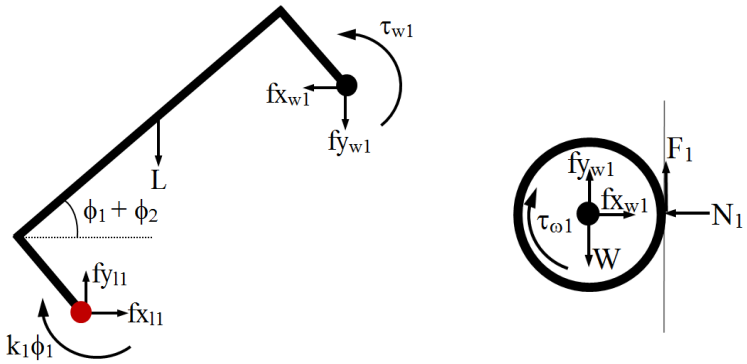

(a) Trunk 1 (b) Wheel 1

Figure 8.4

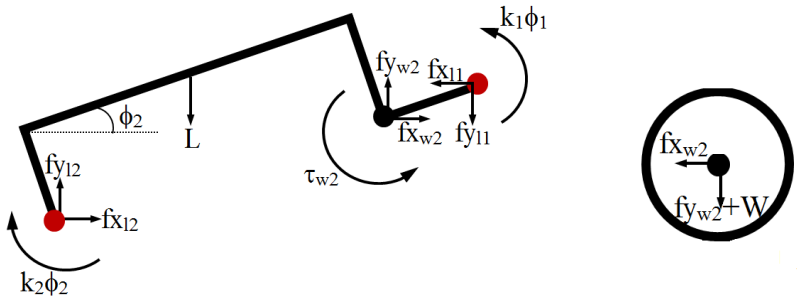

(a) Trunk 2 (b) Wheel 2

Figure 8.5

(b) Module 2

$$
\begin{aligned}
&For\ Trunk\ 2,\\
&fx_{l2} - fx_{l1} + fx_{w2} = 0\\
&fy_{l2} + fy_{w2} - fy_{l1} - L = 0\\
&k_2\phi_2 - k_1\phi_1 + L[(l/2)cos\phi_2 - csin\phi_2]\\
&- fx_{l1}(l + l_0)sin\phi_2 + fy_{l1}(l + l_0)cos\phi_2 - fx_{w2}l - 2\tau_{w2} = 0
\end{aligned}
$$

$$
\begin{aligned}
&For\ Wheel\ 2,\\
&fx_{w2} = 0\\
&fy_{w2} + 2W = 0\\
&\tau_{w2} = 0
\end{aligned}
$$

(c) Module 3

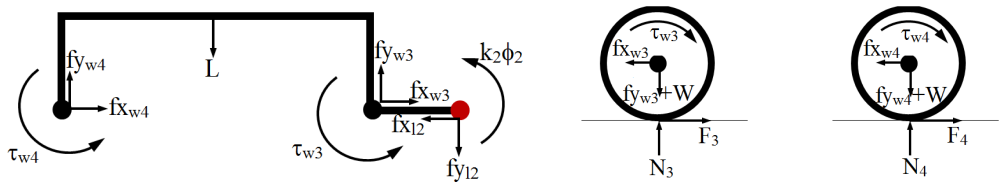

(a) Trunk 3 (b) Wheel 3 (c) Wheel 4

Figure 8.6

For Trunk 3,	*For Wheel* 3,	*For Wheel* 4,
$fx_{l2} - fx_{w3} - fx_{w4} = 0$	$fx_{w3} - 2F_3 = 0$	$fx_{w4} - 2F_4 = 0$
$fy_{w4} + fy_{w3} - fy_{l2} - L = 0$	$fy_{w3} - 2N_3 + 2W = 0$	$fy_{w4} - 2N_4 + 2W = 0$
$-k_2\phi_2 + L(l/2) + fy_{l2}(l + l_0)$	$\tau_{w3} - F_3 r = 0$	$\tau_{w4} - F_4 r = 0$
$- fx_{w3} l - 2\tau_{w3} - 2\tau w4 = 0$		

4. Reduced System of Equations

   (a) For One Link Climbing Case

$$
\begin{aligned}
& N_1 - F_2 - F_3 - F_4 = 0 \\
& 2F_1 + 2N_2 + 2N_3 + 2N_4 - 8W - 3L = 0 \\
& k_1\phi_1 + L[(l/2)cos\phi_1 - csin\phi_1] + (2W - 2F_1)lcos\phi_1 \\
& - 2N_1 lsin\phi_1 - 2\tau_{w1} = 0 \\
& k_2\phi_2 - k_1\phi_1 + (L + 2W - 2F_1)(l + l_0) \\
& + (2W - 2N_2)l - 2\tau_{w2} = 0 \\
& L(l/2) + (2L + 4W - 2F_1 - 2N_2)(l + l_0) + (2W - 2N_3)l \\
& - 2\tau_{w3} - 2\tau_{w4} - k_2\phi_2 = 0 \\
& \tau_{w1} - F_1 r = 0 \\
& \tau_{w2} - F_2 r = 0 \\
& \tau_{w3} - F_3 r = 0 \\
& \tau_{w4} - F_4 r = 0
\end{aligned}
\tag{8.1}
$$

(8.2)

(b) For Two Link Climbing Case

$$
\begin{aligned}
&N_1 - F_3 - F_4 = 0 \\
&2F_1 + 2N_3 + 2N_4 - 8W - 3L = 0 \\
&k_1\phi_1 + L[(l/2)cos(\phi_1 + \phi_2) - csin(\phi_1 + \phi_2)] + \\
&(2W - 2F_1)lcos(\phi_1 + \phi_2) - 2N_1 lsin(\phi_1 + \phi_2) - 2\tau_{w1} = 0 \\
&k_2\phi_2 - k_1\phi_1 + (L + 2W - 2F_1)(l + l_0)cos\phi_2 \\
&+ 2Wlcos\phi_2 - 2N_1(l + l_0)sin\phi_2 = 0 \\
&L(l/2) + (2L + 4W - 2F_1)(l + l_0) + (2W - 2N_3)l - 2\tau_{w3} - 2\tau_{w4} - k_2\phi_2 = 0 \\
&\tau_{w1} - F_1 r = 0 \\
&\tau_{w2} = 0 \\
&\tau_{w3} - F_3 r = 0 \\
&\tau_{w4} - F_4 r = 0
\end{aligned}
\tag{8.3}
\tag{8.4}
$$

Chapter 9

Related Publications

1) A Semi-Active Robot for Steep Obstacle Ascent, IEEE Multi-conference and Systems and Control (MSC), Hyderabad, India, 2013.

2) Wheel Torque Optimization for a Compliant Modular Robot, International and National Conference on Machines and Mechanisms (iNaCOMM), Roorkee, India, 2013.

3) A Compliant Multi-module Robot for Climbing Big Step-like Obstacles, IEEE International Conference of Robotics and Automation (ICRA), Hong Kong, China, 2014.

4) Wheel Torque Optimization for a Compliant Modular Robot, Robotica, submitted.

5) A novel Compliant Modular Robot for climbing and descending big obstacles, Journal of Field Robotics (JFR), submitted.